ACS Energy LETTERS

http://pubs.acs.org/journal/aelccp

LETTER

Switchable Anion Exchange in Polymer-Encapsulated $APbX_3$ Nanocrystals Delivers Stable All-Perovskite White Emitters

Muhammad Imran,*,# Binh T. Mai,# Luca Goldoni, Matilde Cirignano, Houman Bahmani Jalali, Francesco Di Stasio, Teresa Pellegrino,* and Liberato Manna*

Cite This: *ACS Energy Lett.* 2021, 6, 2844−2853

Read Online

ACCESS | Metrics & More | Article Recommendations | Supporting Information

ABSTRACT: We report a one-step synthesis of halide perovskite nanocrystals embedded in amphiphilic polymer (poly(acrylic acid)-*block*-poly(styrene), PAA-*b*-PS) micelles, based on injecting a dimethylformamide solution of PAA-*b*-PS, $PbBr_2$, ABr (A = Cs, formamidinium, or both) and "additive" molecules in toluene. These bifunctional or trifunctional short chain organic molecules improve the nanocrystal−polymer compatibility, increasing the nanocrystal stability against polar solvents and high flux irradiation (the nanocrystals retain almost 80% of their photoluminescence after 1 h of 3.2 w/cm^2 irradiation). If the nanocrystals are suspended in toluene, the coil state of the polymer allows the nanocrystals to undergo halide exchange, enabling emission color tunability. If the nanocrystals are suspended in methanol, or dried as powders, the polymer is in the globule state, and they are inert to halide exchange. By mixing three primary colors we could prepare stable, multicolor emissive samples (for example, white emitting powders) and a UV-to-white color converting layer for light-emitting diodes entirely made of perovskite nanocrystals.

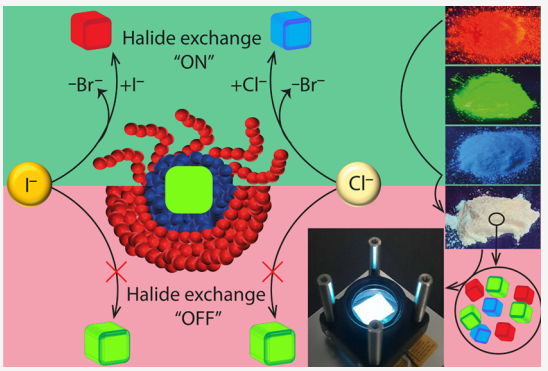

Metal halide perovskite (MHP) nanocrystals (NCs) are promising materials for light emitting technologies.[1−4] NCs with various compositions (AMX_3, A = Cs, CH_3NH_3, or $HC(NH)NH_2$, M = Pb, Sn and X = Cl, Br, I) can be prepared easily,[5−10] and their emission color is tunable across the ultraviolet−visible spectrum and beyond, by alloying, doping, or anion/cation exchange.[6,8,11−14] These NCs are coated with surfactant molecules that stabilize them in nonpolar or moderately polar organic solvents.[15−18] Yet, the NCs have a poor stability against moisture, polar solvents, and long-time exposure to irradiation. Also, when MHP NCs of different emission colors are deposited together in solid films or are mixed in a colloidal suspension, they undergo halide ion exchange. This inter-NCs reactivity limits the use of MHP NCs as multicolor emitters, for example, in white light emission.[3,19−21] So far, white light emission was achieved mainly by blending green emitting perovskite NCs with organic dyes or metal chalcogenides NCs. Similarly, in down-converting white light emitting devices white emission was achieved by combining green emitting perovskite NCs with a commercial UV-LED chip and a nonperovskite based red phosphor.[22−31]

Strategies have been designed to prevent anion exchange and/or to stabilize MHP NCs against polar solvents, including encapsulation of NCs in matrixes made of metal oxides (e.g., $PbSO_4$, SiO_2, TiO_2, Al_2O_3), inorganic salts ($SrBr_2$), a mixture of metal oxides and inorganic salts, metal organic hybrids (e.g., metal organic frameworks), and polymers.[23,24,32−46] Polymers are appealing as they can switch their chains from an extended coil state to a collapsed globule state when the characteristics of the solvent change. In its globule state, a polymer can act as a protecting layer that shields the NCs from their surroundings, making them unreactive. In its coil state, a polymer stretches in solution and partially exposes the NC's surface to the surrounding media, thus allowing a series of chemical reactions with the NCs, hence making them "reactive". The switch from the globule to the coil phase of a

Received: June 14, 2021
Accepted: July 6, 2021

https://doi.org/10.1021/acsenergylett.1c01232
ACS Energy Lett. 2021, 6, 2844−2853

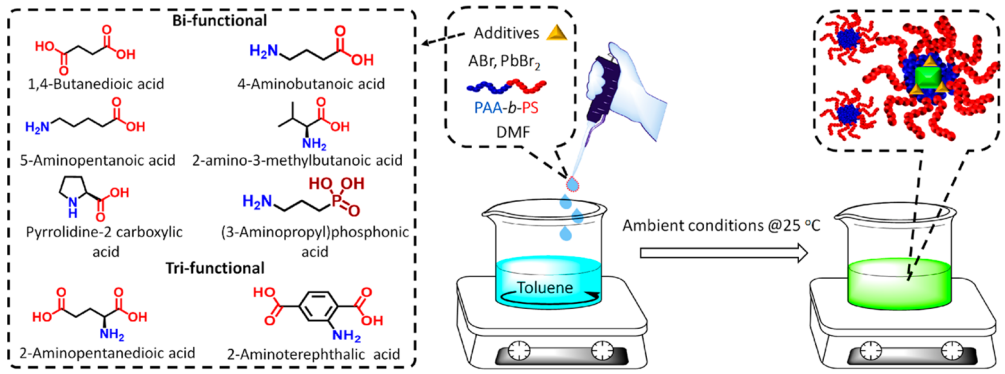

Figure 1. Sketch of the synthesis of $APbX_3$ NCs encapsulated in PAA-*b*-PS micelles (right), along with a set of additive molecules that turned out to be successful to increase the stability of such NCs (left). The screening and role of these molecules are discussed in detail later in this work.

polymer is solvent-dependent and can be properly tuned. This solvent-driven unique feature of certain classes of polymers to reversibly switch the behavior of MHP NCs from unreactive to reactive, especially toward anion exchange reactions, has remained unexplored until now. Polymeric micelles have also been used as templates to synthesize inorganic NCs with low polydispersity and a stable surface coating.[47−50] Polymers with hydrophobic characteristics are ideal choices to protect MHP NCs from polar solvents and have been widely tested in this regard.[51−57] For example, previous studies have shown that embedding $CsPbBr_3$ NCs in different polymeric matrices significantly improves the stability of such NCs.[58] Similarly, various types of polymeric micelles have been exploited as a template to encapsulate, *in situ*, individual MHP NCs.[59−62] A more detailed discussion of these studies, along with a critical discussion and comparison with the present work, is reported in the SI (see also Table S1). From these studies it emerges that the resistance of the NCs against high volume ratio of polar solvents (and especially short-chain alcohols such as methanol) and high flux irradiation is still limited. Also, most of these preparative approaches are not widely accessible and/or scalable, as they often involve various polymerization steps. Overall, the stability of these NCs under operating conditions that are typical for many applications (high humidity, polar solvents, high flux irradiation, etc.) has yet to be proven satisfactory.

We report here an efficient method to encapsulate $APbX_3$ NCs by combining a commercially available diblock copolymer, namely poly(acrylic acid)-*block*-poly(styrene) (PAA-*b*-PS), with short chain "additive molecules" that contain two or more functional groups (for example, carboxylic, phosphonic, amino, or combinations of these). The additive molecules improve the compatibility between the NCs and the block copolymer during the encapsulation process, as they increase the stability of the encapsulated NCs against polar solvents and high flux irradiation. Extensive nuclear magnetic resonance (NMR) analysis on the polymeric micelles encapsulating the NCs proved their core−shell structure, with PAA forming the core of the micelles and PS the outer shell. When the polymer-encapsulated NCs are suspended in nonpolar solvents (for example, toluene), the polymer shell remains in the coil state, and the NCs can undergo halide exchange reactions, allowing color tunability. Instead, when the NCs are dispersed in polar solvents (such as methanol), or dried and stored as powders, the polymer shell is in the globule state, and the surface of the NCs cannot be accessed by chemicals from their surroundings, thereby making them inert toward halide exchange reactions. Based on this property, we could prepare stable multicolor emissive samples retaining their spectral features even after months of storage under air. Such control over the structural and color stability enabled us to prepare white emitting powders fully based on perovskite NCs. The PAA-*b*-PS-encapsulated NCs were very robust against high flux irradiation (3.2 w/cm^2), retaining over 78% of their photoluminescence (PL) efficiency after 1 h of continuous irradiation under such conditions (this can be considered an accelerated stability test). Finally, the white emitting powder was embedded in a polymeric matrix and a UV-to-white color converting layer for light-emitting diodes entirely made of perovskite NCs was fabricated.

The PAA-*b*-PS-encapsulated NCs were prepared under ambient conditions. PAA-*b*-PS with a molar mass of 5000 and 28000 g·mol^{-1}, respectively, was chosen to ensure that the resulting assembled structures are micelles with a PAA core and a PS shell in a nonpolar solvent such as toluene.[63] As additives, we used short organic molecules carrying two or more functional groups: these were either all acidic in nature or a combination of acidic groups and basic (for example, amino) ones (Figure 1; see discussion later). PAA-*b*-PS-encapsulated $APbBr_3$ (A = Cs, formamidinium (FA) or their mixture) NCs were prepared by a ligand assisted reprecipitation route. In a typical synthesis, ABr (CsBr, FABr or their mixture), $PbBr_2$ PAA-*b*-PS, and 5-aminopentanoic acid (APAc) as an additive molecule (one of the best working molecules) were separately dissolved in dimethylformamide (DMF) to form stock solutions. $PbBr_2$ and FABr were dissolved quickly in DMF, while CsBr had a negligible solubility in it (even under sonication at 60 °C). The addition of PAA-*b*-PS to DMF (at a ratio of 1:20 for Cs to PAA) helped to dissolve CsBr completely. Then, equal molar volumes of ABr and $PbBr_2$ stock solutions were mixed with PAA-*b*-PS and APAc stock solutions. This solution was injected dropwise in toluene (a selective solvent for the PS block), triggering at once the formation of polymer micelles and the nucleation and growth of $APbBr_3$ NCs in the micelles. After 20 s, the reaction was quenched by adding excess hexane and the NCs were collected by centrifugation. The supernatant was discarded and the precipitate was redispersed in toluene followed by another round of centrifugation and redispersion in toluene.

The NCs under the transmission electron microscope (TEM) had nearly cubic shapes in all three cases (Figure S1). We carried out dynamic light scattering (DLS) measure-

https://doi.org/10.1021/acsenergylett.1c01232
ACS Energy Lett. 2021, 6, 2844−2853

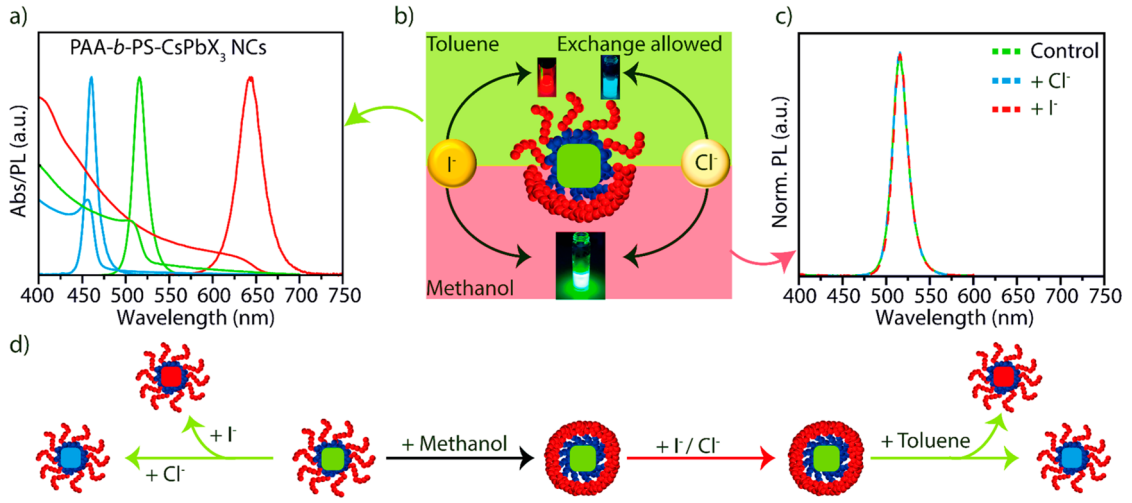

Figure 2. "On demand" color tunability in PAA-*b*-PS-encapsulated $CsPbBr_3$ NCs. (a) Optical absorption and PL spectra of the initial $CsPbBr_3$ NCs sample dispersed in toluene (green curves) and of the corresponding samples upon the addition of either didodecyldimethylammonium chloride (blue curves) or oleylammonium iodide solutions (red curves). The sketch in (b) illustrates the switchable anion exchange mechanism: in toluene dispersions, the polymer shell is open (coil state) and the color tunability is allowed upon halide addition. In methanol, the polymer shell is closed (globule state); hence anion exchange is inhibited and the pristine color is retained. The latter case is illustrated in panel (c) reporting the PL spectra of the initial $CsPbBr_3$ NCs sample and that of the samples after addition of the chloride and iodide salts. (d) Sketches summarizing the halide exchange reactions under the various conditions.

ments on the PAA-*b*-PS-encapsulated $CsPbBr_3$ NCs and on PAA-*b*-PS empty micelles, in toluene. Empty micelles were prepared in the same way as the polymer-encapsulated NCs, except for the addition of metal halide salts (ABr and $PbBr_2$) and additive molecules in the DMF solution. The empty micelles and the NCs had hydrodynamic diameters (d_H) of 48 and 80 nm (weighted by intensity), respectively, with a single peak present in the 1−1000 nm range (Figures S2 and S3). The data for the NC sample exclude the presence of large aggregates of NCs, in agreement with TEM analyses. The d_H values weighted by volume and number were also as small as 51 and 61 nm, confirming the absence of aggregates or large particles (Figures S2 and S3). Similar numbers were found by DLS measurements on PAA-*b*-PS-encapsulated $Cs_{0.5}FA_{0.5}PbBr_3$ and $FAPbBr_3$ NCs (Figures S4 and S5). The polydispersity index (PDI) of the empty micelles and PAA-*b*-PS-encapsulated NCs was in the range of 0.06−0.13, confirming their narrow size distribution (Table S2). Based on X-ray diffraction (XRD, Figure S6a), perovskite was the only phase in all samples. Partial or complete substitution of the A-site cation Cs with the larger FA cations was attested by the shift of the XRD peaks toward lower angles (larger cell) compared to the reference $CsPbBr_3$ pattern (Figure S6b). In toluene, the NCs had emissions centered at 517 nm ($CsPbBr_3$), 527 ($Cs_{0.5}FA_{0.5}PbBr_3$), and 535 nm ($FAPbBr_3$) with 18−22 nm line widths (Figures S6c and S7). PL quantum yield (PLQY) values of the samples (in toluene dispersions) were in the 30−61% range and average PL lifetimes were in the 1.6−36 ns range (Figure S8 and Table S3).

On the PAA-*b*-PS-encapsulated $APbBr_3$ NCs we have the unique chance to reversibly turn on/off anion exchange: when the NCs were dispersed in toluene, in which the polymer is in the coiled state, anion exchange was allowed and the emission color of the NCs was tuned by dosing the halide reagent, didodecyldimethylammonium chloride (DDACl) or oleylammonium iodide (OLAM-I) for the exchange of bromide with chloride or iodide, respectively (Figure 2a,b; see the Experimental Section in the SI for details). When the NCs were dispersed in methanol, in which the polymer is in a globule state (due to the low solubility of the polymer in this solvent), anion exchange was prevented. This is demonstrated on green emitting PAA-*b*-PS-encapsulated $CsPbBr_3$ NCs; see Figure 2b,c and Videos S1 and S2. Even when both chloride and iodide reagents were introduced together in large excess in the methanol dispersion of PAA-*b*-PS-encapsulated $CsPbBr_3$ NCs, the initial PL spectral position and PL line width were retained, thus confirming a complete inhibition of anion exchange (Figure 2c). On the other hand, anion exchange could be easily triggered by adding an excess amount of toluene to open the PS-protecting layer. This is demonstrated by adding the chloride reagent in large excess to the methanol dispersion of PAA-*b*-PS-encapsulated $CsPbBr_3$ NCs: halide exchange did not occur until the addition of toluene (Video S3). We also tested anion exchange reactions on green emitting PAA-*b*-PS-encapsulated NCs using other reagents, such as ZnI_2, which is highly soluble in methanol (as opposed to OLAM-I which is weakly soluble) and has been previously used for halide exchange reactions in toluene dispersions of perovskite NCs.[64] Also in this case, anion exchange was prevented in methanol dispersions (Figure S9-a and Video S4), while it was allowed in toluene (Figure S9-b and Video S4). This proves that the switchable halide exchange behavior of our polymer coated NCs does not depend on the type of halide reagent used and is only related to the coil/globule state of the polymer. The sketches in Figure 2d summarize the halide exchange reactions carried out under the various conditions.

We then assessed the stability of the PAA-*b*-PS-encapsulated NCs in various polar solvents, choosing PAA-*b*-PS-encapsulated $CsPbBr_3$ NCs as a representative system. The toluene dispersion of these NCs was added dropwise to methanol at a volume ratio of 1 to 10 (toluene to methanol) under ambient conditions, to induce the globule state of the PS shell, as discussed earlier. After about 30 s, an excess amount of hexane was added and the NCs dispersion was centrifuged. Then, the supernatant was discarded, the precipitate was redispersed in

https://doi.org/10.1021/acsenergylett.1c01232
ACS Energy Lett. 2021, 6, 2844−2853

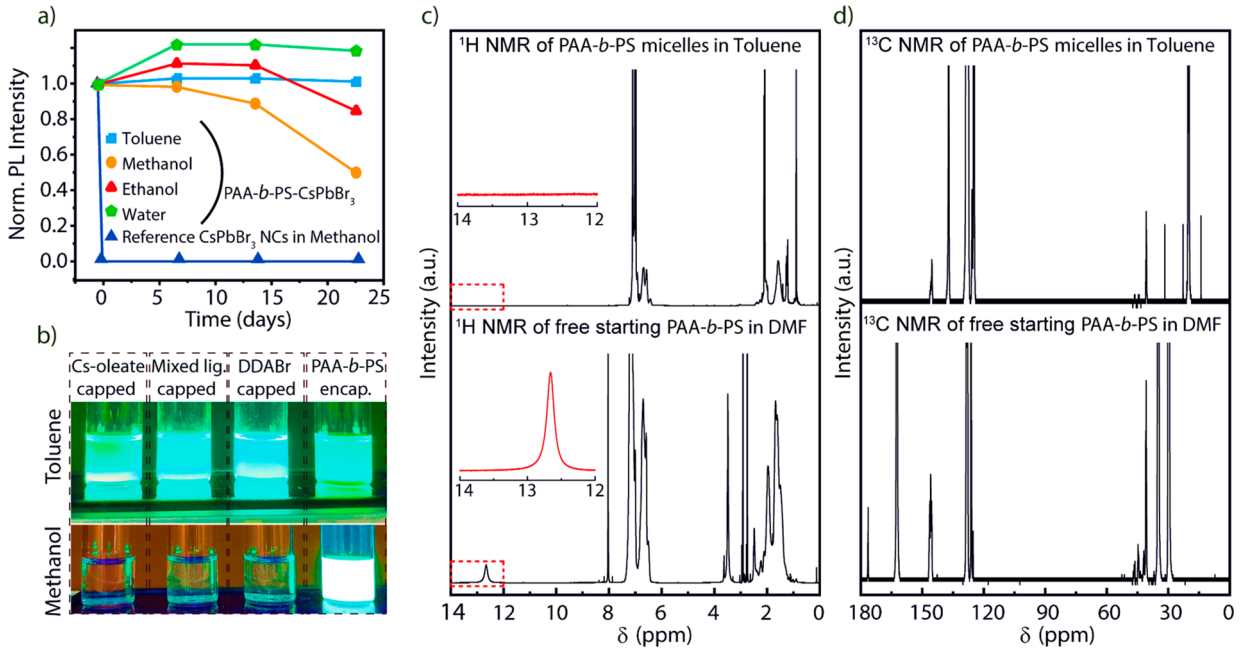

Figure 3. (a) Stability of PAA-*b*-PS-encapsulated $CsPbBr_3$ NCs in different solvents, including toluene, water, ethanol, and methanol in comparison to the "reference" $CsPbBr_3$ NCs over 23 days (the PL spectra of the corresponding samples are reported in Figure S10). The reference $CsPbBr_3$ NCs used for the stability test were synthesized using oleic acid and oleylamine; hence they were not polymer-encapsulated. (b) Photographs of vials containing $CsPbBr_3$NCs capped with different ligands (Cs-oleate,[65] mixed ligands (oleylammonium oleate/bromide)[6], DDABr[66]), and PAA-*b*-PS-encapsulated $CsPbBr_3$ NCs, in toluene and methanol. Panels (c) and (d) report the ^1H and ^{13}C NMR spectra of the free PAA-*b*-PS polymer and the empty PAA-*b*-PS micelles in toluene-d_8 and DMF-d_7, respectively. The empty polymer micelles were prepared in the same way as the polymer-encapsulated NCs, except for the addition of metal halide salts (ABr and $PbBr_2$) and additive molecules in the DMF solution.

the desired polar solvent (methanol, ethanol, water), and the NCs dispersions were stored under ambient conditions to examine their PL stability over time. The PL spectra recorded over time for PAA-*b*-PS-encapsulated $CsPbBr_3$ NCs dispersed in various solvents are reported in Figure S10. The NCs dispersed in toluene and water nearly retained their PL intensity and PL spectral position (Figure S10a,b). In ethanol and methanol, a drop of 18% and 53% in PL intensity was seen after 23 days of aging, while the PL spectral positions remained nearly unchanged (Figure S10c,d). Quantitative data on the drop of PL intensity of the polymer-encapsulated NCs in different solvents are reported in Figure 3a. These are compared with "reference" $CsPbBr_3$ NCs that were synthesized using oleic acid and oleylamine as surfactants (following the method of Protesescu et al.[6]), hence not polymer-encapsulated. The PL from this reference sample was immediately quenched as soon as methanol was added to it. A more extended comparison is reported in Figure 3b: we benchmarked the stability in methanol of the PAA-*b*-PS-encapsulated $CsPbBr_3$ NCs with various NCs which were prepared following published recipes.[6,65,66] Again, these NCs were not polymer-encapsulated but they were coated with various ligands, such as Cs-oleate, mixed ligands (Cs-oleate/oleylammonium bromide), and didodecyldimethylammonium bromide (DDABr capped) and were initially dispersed in toluene. As soon as methanol was added, all the NCs samples lost their PL, except for the polymer-encapsulated one.

We performed detailed high resolution liquid state NMR spectroscopy to assess the structural conformation of the PAA-*b*-PS. The NMR experiments were carried out on the starting free PAA-*b*-PS, empty PAA-*b*-PS micelles, and PAA-*b*-PS-encapsulated NCs. The details on the preparation of all the samples used for NMR experiments are reported in the SI. Heteronuclear Single Quantum Coherence (HSQC) and $^1H-^{13}C$ Heteronuclear Multiple Bond Correlation (HMBC) NMR analyses on the starting free PAA-*b*-PS and empty PAA-*b*-PS micelles in selective (toluene) and nonselective (DMF) solvents; see Figure 3c,d and Figures S11−13. First, the ^1H and ^{13}C NMR analysis on the starting free PAA-*b*-PS in DMF-d_7 evidenced the signals corresponding to both PAA and PS moieties (see Figure 3c,d bottom panel and Figure S11 of SI). The complete ^1H and ^{13}C peak assignment, as well as the HMBC cross correlation peaks, enabled us to unambiguously identify the diagnostic signal (3) in position α to CO (2) of the carboxylic moiety of the PAA component, which does not overlap with the CHs of the PS moiety (see the NMR spectra in DMF in Figure S11A−D). We then carried out the same set of experiments, under identical conditions, on the empty PAA-*b*-PS micelles sample in a toluene-d_8 dispersion. The detailed analysis of the ^1H, ^{13}C, 2D $^1H-^{13}C$, HSQC, and $^1H-^{13}C$ HMBC NMR revealed that the characteristic signals belonging to the PAA component are not detectable (see Figure 3c,d top panel and Figure S12A−D of the SI). On the other hand, the characteristic peaks belonging to the PS component of the polymer could be clearly identified and properly indexed. Here, the inaccessibility to the solvent (responsible for a reduced mobility) of the PAA component of the PAA-*b*-PS micelle is compatible with a model in which PAA forms a rigid core, while PS is present at the outer shell. We further recorded the ^1H NMR spectrum of the PAA-*b*-PS-encapsulated NCs in toluene-d_8 and compared it with the ^1H NMR spectrum of the empty micelles (see Figure S12A,B). The spectrum of the empty PAA-*b*-PS micelles had peak profiles and signal widths

https://doi.org/10.1021/acsenergylett.1c01232
ACS Energy Lett. 2021, 6, 2844−2853

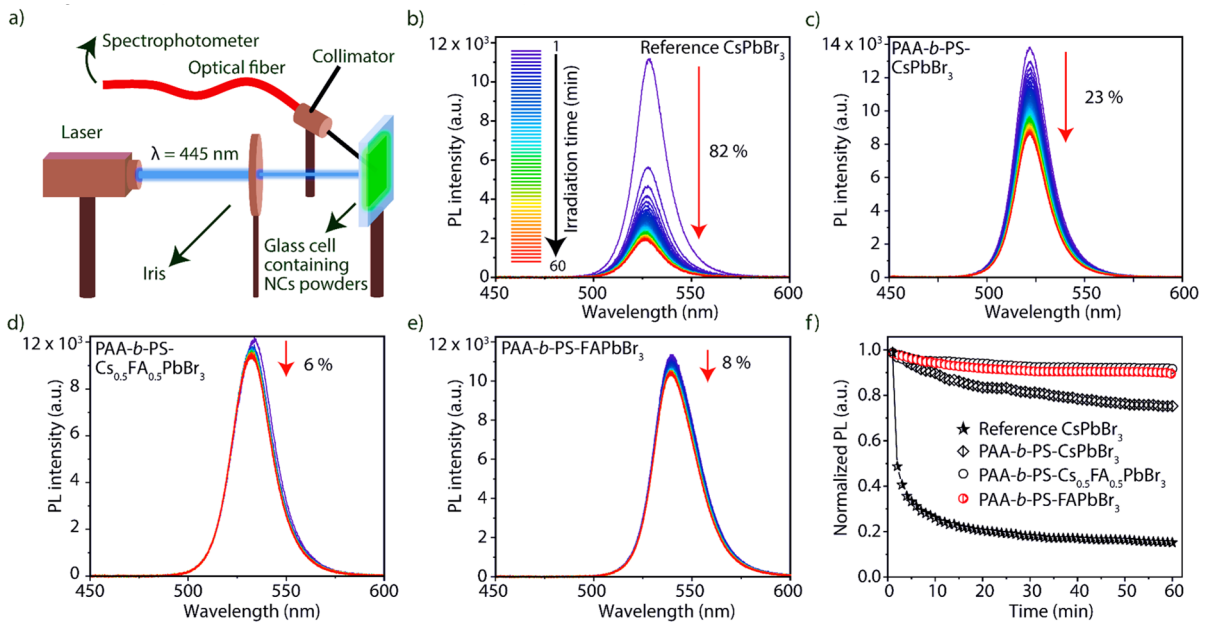

Figure 4. Stability test under high flux irradiation of "reference" $CsPbBr_3$ NCs (synthesized using oleic acid and oleylamine; then mixed with polystyrene) versus PAA-*b*-PS-encapsulated NCs. (a) sketch of the experimental setup; (b) evolution of the PL of the reference $CsPbBr_3$ NCs, evidencing 82% loss of PL intensity over 60 min of continuous exposure to laser irradiation. Over the same time frame, the PL spectra of the PAA-*b*-PS-encapsulated $CsPbBr_3$ (c), $Cs_{0.5}FA_{0.5}PbBr_3$ (d), and $FAPbBr_3$ NCs (e) retained 78%, 94%, and 92% of their initial intensity. (f) Summary of all the data sets for panels (b−e) referred to PL intensity (normalized to the initial PL of each sample).

at half-height that were identical to those of the micelles with the NCs inside, thereby confirming the similar structure of the polymer micelles in both cases. These measurements overall confirm that PAA forms the core of the micelles encapsulating the perovskite NCs, while PS forms the outer shell (see detailed discussion in the NMR section of the SI).

All the samples presented so far were prepared using 5-aminopentanoic acid (APAc), as this molecule led to stable polymer-encapsulated NCs, but other small molecules were also identified as suitable additives. A detailed description of the tests on the various molecules and related discussion are reported in the SI (see also Figures S14−S18 and Table S4). Typical molecules that were tested include hexan-1-amine, hexanoic acid, 2-aminoethanethiol, 4-aminobutanoic acid, 5-aminopentanoic acid, (3-aminopropyl)phosphonic acid, 1,4-butandioic acid, 2-amino-3-hydroxypropanoic acid, pyrrolidine-2-carboxylic acid, 2-amino-3-methylbutanoic acid, 2-amino-5-(diaminomethylideneamino)pentanoic, 2-aminopentanedioic acid, 2-amino-3-sulfhydrylpropanoic acid, 2-amino-3-(1*H*-imidazol-4-yl)propanoic acid, and 2-aminoterphthalic acid. Upon dispersing in methanol, the samples prepared using additive molecules with one functional group (for example, hexan-1-amine, hexanoic acid and even their mixture) significantly lost their PL. On the other hand, the sample prepared using, for example, 5-aminopentanoic acid, which contains two functional groups (carboxylic and amino), remained bright and stable. The results from our tests indicate that effective molecules should be bifunctional or even trifunctional in nature, with either all acidic (carboxylic, phosphonic) groups or a combination of acidic and at most one basic (such as amino) groups. The details about the PL stability of PAA-*b*-PS-encapsulated $FAPbBr_3$ NCs prepared by various additives molecules are summarized in Table S4. The optimal concentration of additive molecule(s) was found to be in the range of 10−15 mM. As a control, when no additive molecules were added, all samples were quickly degraded in methanol (Figures S17 and 18). The mechanism underpinning the increased stability when using certain types of additive molecules is presently not entirely clear. Most likely these molecules partially bind to the surface of the NCs and at the same time they interact with the polymer, ensuring a higher compatibility between the two components. In addition, additive molecules having more than two functional groups might also cross-link the PAA core *via* hydrogen bonding and/or ionic bonding,[67,68] further improving the stability of the PAA-*b*-PS-encapsulated NCs. The relative fraction of these molecules is, however, so low that they cannot be distinguished by NMR or by other techniques against the much dominant signals from the polymer component.

Next, we tested the fluorescence stability of PAA-*b*-PS-encapsulated $APbBr_3$ NCs under high flux photon irradiation. Note that all samples considered for the tests were prepared by blending NCs dispersions in toluene with polystyrene (see the SI for details). PAA-*b*-PS-encapsulated $CsPbBr_3$, $Cs_{0.5}FA_{0.5}PbBr_3$, and $FAPbBr_3$ NCs samples were prepared using APAc as an additive molecule. The "reference" $CsPbBr_3$ NCs prepared *via* a standard colloidal approach[6] and capped with oleylammonium oleate/bromide[69] ligand pairs (see the SI) were then blended with polystyrene and tested in parallel under identical conditions. A sketch of the setup used for the stability test is shown in Figure 4a. A known amount of powders of the reference $CsPbBr_3$ NCs, PAA-*b*-PS-encapsulated $CsPbBr_3$, $Cs_{0.5}FA_{0.5}PbBr_3$, and $FAPbBr_3$ NCs were placed between two glass slides and irradiated continuously under a flux of 3.2 W/cm^2 for 60 min at 445 nm. These high flux irradiation conditions are nearly ten times harsher than the required industrial standards for displays (100−400 mW/cm^2).[70,71] The PL spectra of the reference NCs and the PAA-*b*-PS-encapsulated NCs were monitored by an acquisition every 60 s *via* a software interface. The spectra are reported in Figure

https://doi.org/10.1021/acsenergylett.1c01232
ACS Energy Lett. 2021, 6, 2844−2853

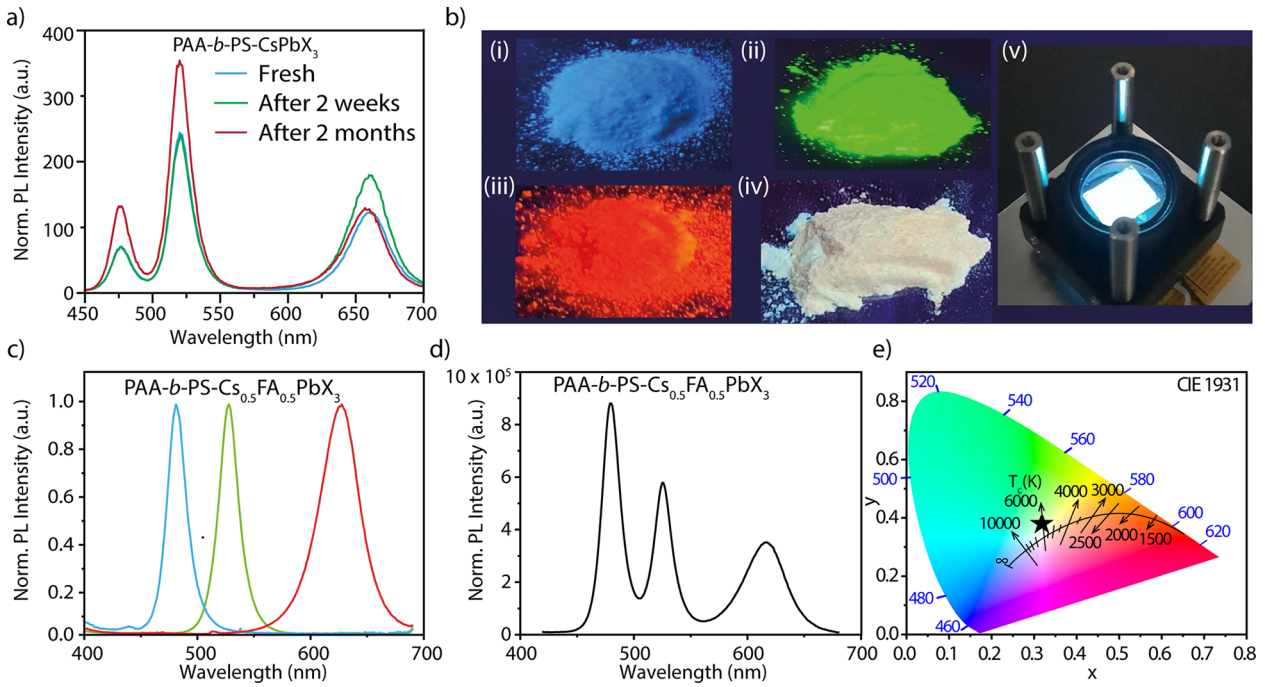

Figure 5. (a) Multicolor fluorescent powders were prepared by mixing the appropriate ratios of PAA-*b*-PS-encapsulated $CsPb(BrCl)_3$, $CsPbBr_3$, and $CsPb(BrI)_3$ NCs powders emitting at 476, 520, and 661 nm, respectively. These powders were prepared from the dried samples, as delivered from the synthesis and, for the blue and red emitting samples, after anion exchange, by grounding with a mortar and pestle in a ceramic crucible. The PL spectra recorded over two months of aging indicate the retention of the PL peaks position. (b) Photos of the separate blue (i), green (ii), and red (iii) emitting powders of PAA-*b*-PS-encapsulated $Cs_{0.5}FA_{0.5}PbX_3$ NCs and their mixture (iv). These powders were prepared instead by ball milling. All photos were taken while irradiating the samples with a UV lamp. (c) The PL spectra of the separate powders reported in panel (b) (i–iii) with emission centered at 481, 527, and 625 nm for the blue, green, and red samples, respectively. The red, green, and blue powders reported in panel (b) (i–iii) were then blended in appropriate ratios with a water solution of poly(vinyl alcohol) (PVA) to prepare white emitting films for the LED. Panels (d) and (e) show the PL spectra and corresponding CIE coordinates of the obtained white emitting films, respectively. A photograph of a white LED under operational conditions is reported in Panel (b) (v). The device structure for the UV-to-white color converting layer is reported in Figure S23.

4b–e and the drop of PL intensities versus irradiation time are reported in Figure 4f. The reference $CsPbBr_3$ sample lost a significant fraction of its PL in the first minute, which further dropped down to 18% of its initial intensity after 60 min of exposure to the laser (i.e., a PL loss of 82%). In comparison, over the same time frame, the PAA-*b*-PS-encapsulated $CsPbBr_3$, $Cs_{0.5}FA_{0.5}PbBr_3$, and $FAPbBr_3$ NC samples lost 23%, 6%, and 8% of their initial PL intensity, respectively, demonstrating their improved stability.

We also tested the effect of an alternative molecule (phenethylammonium, PEABr, which contains only one functional group) on the stability of NCs against high flux radiation. A PAA-*b*-PS-encapsulated $Cs_{0.5}FA_{0.5}PbBr_3$ NCs sample prepared using PEABr was irradiated continuously under a flux of 3.2 W/cm^2 for 60 min at 445 nm. The sample lost 56% of its initial PL intensity after 60 min of exposure to the laser (Figure S19a), that is, a much bigger loss compared to the sample prepared with APAc and discussed earlier (6%, Figure 4d). Similarly, upon dispersion in methanol, the sample prepared using PEABr evidenced a bigger drop in the PL intensity compared to the sample prepared with APAc (Figure S19b).

Our empirical conclusions are the following: to prepare polymer-encapsulated NCs possessing stable optical features under high flux irradiation conditions and which additionally retain their PL against polar solvents (such as methanol), the requested additive molecules need to have more than one functional group. For example, they need to have two or more acidic (carboxylic, phosphonic) groups, or a combination of acidic and basic (such as amino) groups.

Taking advantage of the enhanced stability and color tunability on demand of these NCs, we prepared multicolored emissive samples. We prepared first the green emitting PAA-*b*-PS-encapsulated $CsPbBr_3$ NCs. The red and blue emitting samples were obtained from them by anion exchange in toluene. Once the desired emission color was reached, the polymer shell was "closed" by adding a mixture of methanol and hexane, followed by centrifugation, solution drying, and grounding with a mortar and pestle in a ceramic crucible (see details in the SI). The different powders were then mixed in an appropriate ratio to get a multicolor emitting product that nearly retained the emitting features of the individual components over months of storage under ambient conditions (Figure 5a). Interestingly, the $CsPbI_3$ NCs, which are prone to a phase transition to a nonemitting yellow phase and need additional surface or structural engineering for stability,[12,72–74] were instead stable in the perovskite phase when polymer coated. Inspired by the retention of the emission color and by the excellent stability of the multicolor powders, we then proceeded to prepare a white emitting powder by combining three primary colors (red, green, and blue), fully based on halide perovskite NCs. The A-site cation-dependent color tunability of PAA-*b*-PS-encapsulated $APbBr_3$ NCs in the range of 515 to 540 nm gave us access to the pure green emission range (525–535 nm). Therefore, we used PAA-*b*-PS-encapsulated $Cs_{0.5}FA_{0.5}PbBr_3$ NCs samples considering their

https://doi.org/10.1021/acsenergylett.1c01232
ACS Energy Lett. 2021, 6, 2844–2853

nearly pure green emission features. The PAA-*b*-PS-encapsulated $Cs_{0.5}FA_{0.5}PbBr_3$ NCs samples were prepared using 4-aminobutanoic acid as an additive molecule while all the other reaction conditions, including concentration of the precursor solutions and of the polymer, were kept the same. TEM images of the pristine green emitting NCs and of the samples after anion exchange reaction (blue and red emitting NCs) are reported in Figure S20. The blue and red samples were derived from the green emitting sample by halide exchange, similarly to the procedure previously described for the PAA-*b*-PS-encapsulated $CsPbX_3$ NCs. The PAA-*b*-PS-encapsulated $Cs_{0.5}FA_{0.5}PbX_3$ NCs with desired emission color in toluene dispersion were mixed with poly(methyl methacrylate), known to be an organic glass and suitable for display applications. Then, the polymer shell encapsulating the NCs was closed by adding a methanol/hexane mixture. The precipitate was collected by centrifugation and the dried in a vacuum oven at 40 °C overnight. The dried precipitates were individually ball milled to get the fine powders (see the details in the SI).

The photographs of the powders after ball milling are reported in Figure 5b (i–iii) and the PL spectra recorded from the individual powders are reported in Figure 5c. The PL peak position was centered at 625, 527, and 481 nm for the red, green, and blue NCs powders, respectively. These powders were combined in appropriate ratios to get a white emitting sample. The resulting powder showed nearly white emission under UV-lamp irradiation (Figure 5b (iv), $x = 0.31$ and $y = 0.38$, pure white would be $x = 0.33$ and $y = 0.33$). The PL spectrum recorded on the white emitting powder is reported in Figure S21 and the CIE coordinates are reported in Figure S22. The comparison of the spectral features of the powders before and after mixing and over aging is reported in Figure S21: The individual PL peak positions did not shift after mixing and remained unchanged after 4 weeks of aging under ambient conditions.

The inhibition of halide exchange in the solid matrix further motivated us to fabricate a fully halide perovskite UV-to-white color converting layer combined with a commercial LED. The white emitting films were prepared by blending red, green, and blue powders (reported in Figure 5b (i–iii)) with a water solution of poly(vinyl alcohol) and the sample was drop-cast on quartz substrate (see the details in the SI). The obtained emitting perovskite-PVA film was then placed on a 365 nm LED (maximum power of 1 W) which was used for excitation. A 425 nm long pass filter (Thorlabs) was then placed onto the PVA film to remove the UV excitation light (see Figure S23). The final device featured white emission (Figure 5b (v)) with a conversion ratio of 15% (i.e., 100 mW of 365 nm excitation was converted into 15 mW of white light). The PL spectra and corresponding CIE coordinates of the NC-PVA film used for the white LED are reported in Figure 5d,e.

In conclusion, we have reported an effective *in situ* method to prepare polymer-encapsulated halide perovskite nanocrystals in which we can switch their reactivity toward anion exchange "on demand" by simply changing the polarity of the solvent. The method uses suitable additive molecules that improve the optical stability of the nanocrystals. When protected from anion exchange (for example, when dispersed in polar solvents, or as dried powders), nanocrystals emitting at different colors can be mixed together and the resulting sample preserves the multicolor emission over time. Such color stable samples were further used to prepare fully halide perovskite-based nearly white emitters (and also a white light emitting device based on UV-to-white color converting layer) by simply mixing three primary colors. This unique set of properties, together with a high stability against polar solvents and high-flux irradiation, makes them appealing for a wide range of applications. This method should be easily extendable to other metal halide nanocrystals.

■ ASSOCIATED CONTENT

Supporting Information

The Supporting Information is available free of charge at https://pubs.acs.org/doi/10.1021/acsenergylett.1c01232.

Video S1: Switchable halide exchange using oleylammonium iodide (AVI)

Video S2: Switchable halide exchange using DDACl (AVI)

Video S3: Triggering halide exchange using DDACl by opening the PS-protecting layer with toluene (AVI)

Video S4: Switchable halide exchange using zinc iodide (MP4)

Materials and methods, extended literature review, table of comparison of key features, TEM, DLS, XRD, and NMR analyses, role of various additives on the stability of perovskite NCs in polar solvents, optical absorption and table of optical properties, PL lifetimes, and PL decay curves, switchable halide exchange reactions, aging tests, synthesis and photographs of PAA-*b*-PS-encapsulated $FAPbBr_3$ NCs, additional data on emitting powders and on the white light emitting layer preparation (PDF)

■ AUTHOR INFORMATION

Corresponding Authors

Muhammad Imran − *Nanochemistry, Istituto Italiano di Tecnologia, 16163 Genova, Italy;* orcid.org/0000-0001-7091-6514; Email: muhammad.imran@iit.it

Teresa Pellegrino − *Nanomaterials for Biomedical Applications, Istituto Italiano di Tecnologia, 16163 Genova, Italy;* orcid.org/0000-0001-5518-1134; Email: teresa.pellegrino@iit.it

Liberato Manna − *Nanochemistry, Istituto Italiano di Tecnologia, 16163 Genova, Italy;* orcid.org/0000-0003-4386-7985; Email: liberato.manna@iit.it

Authors

Binh T. Mai − *Nanomaterials for Biomedical Applications, Istituto Italiano di Tecnologia, 16163 Genova, Italy;* orcid.org/0000-0002-3418-0658

Luca Goldoni − *Analytical Chemistry Lab, Istituto Italiano di Tecnologia, 16163 Genova, Italy*

Matilde Cirignano − *Photonic Nanomaterials, Istituto Italiano di Tecnologia, 16163 Genova, Italy; Dipartimento di Chimica e Chimica Industriale, Universitàdegli Studi di Genova, 16146 Genova, Italy*

Houman Bahmani Jalali − *Photonic Nanomaterials, Istituto Italiano di Tecnologia, 16163 Genova, Italy;* orcid.org/0000-0001-7212-9098

Francesco Di Stasio − *Photonic Nanomaterials, Istituto Italiano di Tecnologia, 16163 Genova, Italy;* orcid.org/0000-0002-2079-3322

Complete contact information is available at: https://pubs.acs.org/10.1021/acsenergylett.1c01232

Author Contributions

M.I., B.T.M., T.P, and L.M. conceived the idea. M.I. designed and executed the experiments with the help of B.T.M. F.D.S. and H.B.J. performed the PLQY and PL lifetimes measurements and tested the stability of nanocrystals under laser irradiation. M.C. and M.I. prepared the nanocrystal powders and white emitting films for LED. F.D.S. assembled the LED device and performed measurements. L.G. performed NMR experiments. M.I. and L.M. prepared the initial draft which was further improved through feedback from all the authors.

Author Contributions

[#]M.I. and B.T.M. contributed equally to this work.

Notes

The authors declare the following competing financial interest(s): M.I., B.T.M., F.D.S., T.P., and L.M. are inventors on patent application IT 102021000005213 that covers the synthesis of the polymer-encapsulated particles and their properties.

■ ACKNOWLEDGMENTS

F.D.S, M.C., and H.B.J. acknowledge support from the European research council project NANOLED (ERC-StG 851794). T.P. acknowledges funding support from the European Research Council (starting grant ICARO, contract no. 678109).

■ REFERENCES

(1) Quan, L. N.; Rand, B. P.; Friend, R. H.; Mhaisalkar, S. G.; Lee, T.-W.; Sargent, E. H. Perovskites for next-generation optical sources. *Chem. Rev.* **2019**, *119*, 7444−7477.

(2) Dey, A.; Ye, J.; De, A.; Debroye, E.; Ha, S. K.; Bladt, E.; Kshirsagar, A. S.; Wang, Z.; Yin, J.; Wang, Y. State of the Art and Prospects for Halide Perovskite Nanocrystals. *ACS Nano* **2021**, DOI: 10.1021/acsnano.0c08903.

(3) Liu, X.-K.; Xu, W.; Bai, S.; Jin, Y.; Wang, J.; Friend, R. H.; Gao, F. Metal halide perovskites for light-emitting diodes. *Nat. Mater.* **2021**, *20*, 10.

(4) Gandini, M.; Villa, I.; Beretta, M.; Gotti, C.; Imran, M.; Carulli, F.; Fantuzzi, E.; Sassi, M.; Zaffalon, M.; Brofferio, C.; et al. Efficient, fast and reabsorption-free perovskite nanocrystal-based sensitized plastic scintillators. *Nat. Nanotechnol.* **2020**, *15*, 462−468.

(5) Kovalenko, M. V.; Protesescu, L.; Bodnarchuk, M. I. Properties and potential optoelectronic applications of lead halide perovskite nanocrystals. *Science* **2017**, *358*, 745−750.

(6) Protesescu, L.; Yakunin, S.; Bodnarchuk, M. I.; Krieg, F.; Caputo, R.; Hendon, C. H.; Yang, R. X.; Walsh, A.; Kovalenko, M. V. Nanocrystals of cesium lead halide perovskites ($CsPbX_3$, X= Cl, Br, and I): novel optoelectronic materials showing bright emission with wide color gamut. *Nano Lett.* **2015**, *15*, 3692−3696.

(7) Akkerman, Q. A.; Rainò, G.; Kovalenko, M. V.; Manna, L. Genesis, challenges and opportunities for colloidal lead halide perovskite nanocrystals. *Nat. Mater.* **2018**, *17*, 394−405.

(8) Nedelcu, G.; Protesescu, L.; Yakunin, S.; Bodnarchuk, M. I.; Grotevent, M. J.; Kovalenko, M. V. Fast anion-exchange in highly luminescent nanocrystals of cesium lead halide perovskites ($CsPbX_3$, X= Cl, Br, I). *Nano Lett.* **2015**, *15*, 5635−5640.

(9) Shamsi, J.; Urban, A. S.; Imran, M.; De Trizio, L.; Manna, L. Metal halide perovskite nanocrystals: synthesis, post-synthesis modifications, and their optical properties. *Chem. Rev.* **2019**, *119*, 3296−3348.

(10) Fu, Y.; Zhu, H.; Chen, J.; Hautzinger, M. P.; Zhu, X.-Y.; Jin, S. Metal halide perovskite nanostructures for optoelectronic applications and the study of physical properties. *Nat. Rev. Mater.* **2019**, *4*, 169−188.

(11) Akkerman, Q. A.; D'Innocenzo, V.; Accornero, S.; Scarpellini, A.; Petrozza, A.; Prato, M.; Manna, L. Tuning the optical properties of cesium lead halide perovskite nanocrystals by anion exchange reactions. *J. Am. Chem. Soc.* **2015**, *137*, 10276−10281.

(12) Lu, C.-H.; Biesold-McGee, G. V.; Liu, Y.; Kang, Z.; Lin, Z. Doping and ion substitution in colloidal metal halide perovskite nanocrystals. *Chem. Soc. Rev.* **2020**, *49*, 4953−5007.

(13) Imran, M.; Ramade, J.; Di Stasio, F.; De Franco, M.; Buha, J.; Van Aert, S.; Goldoni, L.; Lauciello, S.; Prato, M.; Infante, I.; et al. Alloy $CsCd_xPb_{1-x}Br_3$ Perovskite Nanocrystals: The Role of Surface Passivation in Preserving Composition and Blue Emission. *Chem. Mater.* **2020**, *32*, 10641−10652.

(14) Imran, M.; Caligiuri, V.; Wang, M.; Goldoni, L.; Prato, M.; Krahne, R.; De Trizio, L.; Manna, L. Benzoyl halides as alternative precursors for the colloidal synthesis of lead-based halide perovskite nanocrystals. *J. Am. Chem. Soc.* **2018**, *140*, 2656−2664.

(15) Yang, D.; Li, X.; Zeng, H. Surface chemistry of all inorganic halide perovskite nanocrystals: passivation mechanism and stability. *Adv. Mater. Interfaces* **2018**, *5*, 1701662.

(16) Zito, J.; Infante, I. The Future of Ligand Engineering in Colloidal Semiconductor Nanocrystals. *Acc. Chem. Res.* **2021**, *54*, 1555−1564.

(17) Smock, S. R.; Chen, Y.; Rossini, A. J.; Brutchey, R. L. The surface chemistry and structure of colloidal lead halide perovskite nanocrystals. *Acc. Chem. Res.* **2021**, *54*, 707−718.

(18) Xue, J.; Wang, R.; Yang, Y. The surface of halide perovskites from nano to bulk. *Nat. Rev. Mater.* **2020**, *5*, 809−827.

(19) Bidikoudi, M.; Fresta, E.; Costa, R. White perovskite based lighting devices. *Chem. Commun.* **2018**, *54*, 8150−8169.

(20) Chang, S.; Bai, Z.; Zhong, H. In situ fabricated perovskite nanocrystals: a revolution in optical materials. *Adv. Opt. Mater.* **2018**, *6*, 1800380.

(21) Brennan, M. C.; Ruth, A.; Kamat, P. V.; Kuno, M. Photoinduced anion segregation in mixed halide perovskites. *Trends Chem.* **2020**, *2*, 282−301.

(22) Li, X.; Wu, Y.; Zhang, S.; Cai, B.; Gu, Y.; Song, J.; Zeng, H. $CsPbX_3$ quantum dots for lighting and displays: room-temperature synthesis, photoluminescence superiorities, underlying origins and white light-emitting diodes. *Adv. Funct. Mater.* **2016**, *26*, 2435−2445.

(23) Sun, C.; Zhang, Y.; Ruan, C.; Yin, C.; Wang, X.; Wang, Y.; Yu, W. W. Efficient and stable white LEDs with silica-coated inorganic perovskite quantum dots. *Adv. Mater.* **2016**, *28*, 10088−10094.

(24) Yoon, H. C.; Kang, H.; Lee, S.; Oh, J. H.; Yang, H.; Do, Y. R. Study of perovskite QD down-converted LEDs and six-color white LEDs for future displays with excellent color performance. *ACS Appl. Mater. Interfaces* **2016**, *8*, 18189−18200.

(25) Pathak, S.; Sakai, N.; Wisnivesky Rocca Rivarola, F.; Stranks, S. D.; Liu, J.; Eperon, G. E.; Ducati, C.; Wojciechowski, K.; Griffiths, J. T.; Haghighirad, A. A. Perovskite crystals for tunable white light emission. *Chem. Mater.* **2015**, *27*, 8066−8075.

(26) Huang, H.; Chen, B.; Wang, Z.; Hung, T. F.; Susha, A. S.; Zhong, H.; Rogach, A. L. Water resistant $CsPbX_3$ nanocrystals coated with polyhedral oligomeric silsesquioxane and their use as solid state luminophores in all-perovskite white light-emitting devices. *Chem. Sci.* **2016**, *7*, 5699−5703.

(27) Yao, E. P.; Yang, Z.; Meng, L.; Sun, P.; Dong, S.; Yang, Y.; Yang, Y. High-brightness blue and white leds based on inorganic perovskite nanocrystals and their composites. *Adv. Mater.* **2017**, *29*, 1606859.

(28) Huang, C.-Y.; Huang, S.-J.; Liu, M.-H. M. Hybridization of $CsPbBr_{1.5}I_{1.5}$ perovskite quantum dots with 9, 9-dihexylfluorene co-oligomer for white electroluminescence. *Org. Electron.* **2017**, *44*, 6−10.

(29) Chang, Y.; Yoon, Y. J.; Li, G.; Xu, E.; Yu, S.; Lu, C.-H.; Wang, Z.; He, Y.; Lin, C. H.; Wagner, B. K. All-inorganic perovskite nanocrystals with a stellar set of stabilities and their use in white light-emitting diodes. *ACS Appl. Mater. Interfaces* **2018**, *10*, 37267−37276.

(30) Xuan, T.; Huang, J.; Liu, H.; Lou, S.; Cao, L.; Gan, W.; Liu, R.-S.; Wang, J. Super-hydrophobic cesium lead halide perovskite quantum dot-polymer composites with high stability and luminescent

efficiency for wide color gamut white light-emitting diodes. *Chem. Mater.* **2019**, *31*, 1042−1047.
(31) Jang, J.; Kim, Y. H.; Park, S.; Yoo, D.; Cho, H.; Jang, J.; Jeong, H. B.; Lee, H.; Yuk, J. M.; Park, C. B. Extremely Stable Luminescent Crosslinked Perovskite Nanoparticles under Harsh Environments over 1.5 Years. *Adv. Mater.* **2021**, *33*, 2005255.
(32) Bose, R.; Yin, J.; Zheng, Y.; Yang, C.; Gartstein, Y. N.; Bakr, O. M.; Malko, A. V.; Mohammed, O. F. Gentle Materials Need Gentle Fabrication: Encapsulation of Perovskites by Gas-Phase Alumina Deposition. *J. Phys. Chem. Lett.* **2021**, *12*, 2348−2357.
(33) Palei, M.; Imran, M.; Biffi, G.; Manna, L.; Di Stasio, F.; Krahne, R. Robustness to High Temperatures of Al_2O_3-Coated $CsPbBr_3$ Nanocrystal Thin Films with High-Photoluminescence Quantum Yield for Light Emission. *ACS Appl. Nano Mater.* **2020**, *3*, 8167−8175.
(34) An, M. N.; Park, S.; Brescia, R.; Lutfullin, M.; Sinatra, L.; Bakr, O. M.; De Trizio, L.; Manna, L. Low-Temperature Molten Salts Synthesis: $CsPbBr_3$ Nanocrystals with High Photoluminescence Emission Buried in Mesoporous SiO_2. *ACS Energy Lett.* **2021**, *6*, 900−907.
(35) Pan, S.; Chen, Y.; Wang, Z.; Harn, Y.-W.; Yu, J.; Wang, A.; Smith, M. J.; Li, Z.; Tsukruk, V. V.; Peng, J. Strongly-ligated perovskite quantum dots with precisely controlled dimensions and architectures for white light-emitting diodes. *Nano Energy* **2020**, *77*, 105043.
(36) Ercan, E.; Tsai, P.-C.; Chen, J.-Y.; Lam, J.-Y.; Hsu, L.-C.; Chueh, C.-C.; Chen, W.-C. Stretchable and ambient stable perovskite/polymer luminous hybrid Nanofibers of multicolor fiber mats and their white LED applications. *ACS Appl. Mater. Interfaces* **2019**, *11*, 23605−23615.
(37) Zhang, H.; Wang, X.; Liao, Q.; Xu, Z.; Li, H.; Zheng, L.; Fu, H. Embedding perovskite nanocrystals into a polymer matrix for tunable luminescence probes in cell imaging. *Adv. Funct. Mater.* **2017**, *27*, 1604382.
(38) Zhong, Q.; Liu, J.; Chen, S.; Li, P.; Chen, J.; Guan, W.; Qiu, Y.; Xu, Y.; Cao, M.; Zhang, Q. Highly Stable $CsPbX_3/PbSO_4$ Core/Shell Nanocrystals Synthesized by a Simple Post-Treatment Strategy. *Adv. Opt. Mater.* **2021**, *9*, 2001763.
(39) Ravi, V. K.; Scheidt, R. A.; Nag, A.; Kuno, M.; Kamat, P. V. To exchange or not to exchange. Suppressing anion exchange in cesium lead halide perovskites with $PbSO_4$-oleate capping. *ACS Energy Lett.* **2018**, *3*, 1049−1055.
(40) Loiudice, A.; Strach, M.; Saris, S.; Chernyshov, D.; Buonsanti, R. Universal oxide shell growth enables in situ structural studies of perovskite nanocrystals during the anion exchange reaction. *J. Am. Chem. Soc.* **2019**, *141*, 8254−8263.
(41) Loiudice, A.; Saris, S.; Oveisi, E.; Alexander, D. T.; Buonsanti, R. $CsPbBr_3$ QD/AlO_x inorganic nanocomposites with exceptional stability in water, light, and heat. *Angew. Chem., Int. Ed.* **2017**, *56*, 10696−10701.
(42) Rainò, G.; Landuyt, A.; Krieg, F.; Bernasconi, C.; Ochsenbein, S. T.; Dirin, D. N.; Bodnarchuk, M. I.; Kovalenko, M. V. Underestimated effect of a polymer matrix on the light emission of single $CsPbBr_3$ nanocrystals. *Nano Lett.* **2019**, *19*, 3648−3653.
(43) Baranov, D.; Caputo, G.; Goldoni, L.; Dang, Z.; Scarfiello, R.; De Trizio, L.; Portone, A.; Fabbri, F.; Camposeo, A.; Pisignano, D. Transforming colloidal Cs_4PbBr_6 nanocrystals with poly (maleic anhydride-alt-1-octadecene) into stable $CsPbBr_3$ perovskite emitters through intermediate heterostructures. *Chem. Sci.* **2020**, *11*, 3986−3995.
(44) Ushakova, E. V.; Cherevkov, S. A.; Sokolova, A. V.; Li, Y.; Azizov, R. R.; Baranov, M. A.; Kurdyukov, D. A.; Yu Stovpiaga, E.; Golubev, V. G.; Rogach, A. L. Stable luminescent composite microspheres based on porous silica with embedded $CsPbBr_3$ perovskite nanocrystals. *ChemNanoMat* **2020**, *6*, 1080−1085.
(45) Lu, Z.; Li, Y.; Qiu, W.; Rogach, A. L.; Nagl, S. Composite films of $CsPbBr_3$ perovskite nanocrystals in a hydrophobic fluoropolymer for temperature imaging in digital microfluidics. *ACS Appl. Mater. Interfaces* **2020**, *12*, 19805−19812.
(46) Ravi, V. K.; Scheidt, R. A.; DuBose, J.; Kamat, P. V. Hierarchical arrays of cesium lead halide perovskite nanocrystals through electrophoretic deposition. *J. Am. Chem. Soc.* **2018**, *140*, 8887−8894.
(47) Pang, X.; Zhao, L.; Han, W.; Xin, X.; Lin, Z. A general and robust strategy for the synthesis of nearly monodisperse colloidal nanocrystals. *Nat. Nanotechnol.* **2013**, *8*, 426.
(48) Pileni, M.-P. The role of soft colloidal templates in controlling the size and shape of inorganic nanocrystals. *Nat. Mater.* **2003**, *2*, 145−150.
(49) Müllner, M.; Lunkenbein, T.; Breu, J.; Caruso, F.; Müller, A. H. Template-directed synthesis of silica nanowires and nanotubes from cylindrical core-shell polymer brushes. *Chem. Mater.* **2012**, *24*, 1802−1810.
(50) Li, F.; Wang, K.; Deng, N.; Xu, J.; Yi, M.; Xiong, B.; Zhu, J. Self-Assembly of Polymer End-Tethered Gold Nanorods into Two-Dimensional Arrays with Tunable Tilt Structures. *ACS Appl. Mater. Interfaces* **2021**, *13*, 6566−6574.
(51) Meyns, M.; Perálvarez, M.; Heuer-Jungemann, A.; Hertog, W.; Ibáñez, M.; Nafria, R.; Genç, A.; Arbiol, J.; Kovalenko, M. V.; Carreras, J. Polymer-enhanced stability of inorganic perovskite nanocrystals and their application in color conversion LEDs. *ACS Appl. Mater. Interfaces* **2016**, *8*, 19579−19586.
(52) Vijila, C. M.; Kumar, K. R.; Jayaraj, M. Stokes shift engineered, stable core-shell perovskite nanoparticle-Poly (methyl methacrylate) composites with high photoluminescence quantum yield. *Opt. Mater.* **2019**, *94*, 241−248.
(53) Wu, H.; Wang, S.; Cao, F.; Zhou, J.; Wu, Q.; Wang, H.; Li, X.; Yin, L.; Yang, X. Ultrastable inorganic perovskite nanocrystals coated with a thick long-chain polymer for efficient white light-emitting diodes. *Chem. Mater.* **2019**, *31*, 1936−1940.
(54) Di, D.; Musselman, K. P.; Li, G.; Sadhanala, A.; Ievskaya, Y.; Song, Q.; Tan, Z.-K.; Lai, M. L.; MacManus-Driscoll, J. L.; Greenham, N. C. Size-dependent photon emission from organometal halide perovskite nanocrystals embedded in an organic matrix. *J. Phys. Chem. Lett.* **2015**, *6*, 446−450.
(55) Huang, S.; Zhang, T.; Jiang, C.; Qi, R.; Luo, C.; Chen, Y.; Lin, H.; Travas-Sejdic, J.; Peng, H. Luminescent $CH_3NH_3PbBr_3$/β-Cyclodextrin Core/Shell Nanodots with Controlled Size and Ultrastability through Host-Guest Interactions. *ChemNanoMat* **2019**, *5*, 1311−1316.
(56) Ko, J.; Ma, K.; Joung, J. F.; Park, S.; Bang, J. Ligand-Assisted Direct Photolithography of Perovskite Nanocrystals Encapsulated with Multifunctional Polymer Ligands for Stable, Full-Colored, High-Resolution Displays. *Nano Lett.* **2021**, *21*, 2288−2295.
(57) Wang, S.; Du, L.; Jin, Z.; Xin, Y.; Mattoussi, H. Enhanced Stabilization and Easy Phase Transfer of $CsPbBr_3$ Perovskite Quantum Dots Promoted by High-Affinity Polyzwitterionic Ligands. *J. Am. Chem. Soc.* **2020**, *142*, 12669−12680.
(58) Raja, S. N.; Bekenstein, Y.; Koc, M. A.; Fischer, S.; Zhang, D.; Lin, L.; Ritchie, R. O.; Yang, P.; Alivisatos, A. P. Encapsulation of perovskite nanocrystals into macroscale polymer matrices: enhanced stability and polarization. *ACS Appl. Mater. Interfaces* **2016**, *8*, 35523−35533.
(59) Hou, S.; Guo, Y.; Tang, Y.; Quan, Q. Synthesis and stabilization of colloidal perovskite nanocrystals by multidentate polymer micelles. *ACS Appl. Mater. Interfaces* **2017**, *9*, 18417−18422.
(60) He, Y.; Yoon, Y. J.; Harn, Y. W.; Biesold-McGee, G. V.; Liang, S.; Lin, C. H.; Tsukruk, V. V.; Thadhani, N.; Kang, Z.; Lin, Z. Unconventional route to dual-shelled organolead halide perovskite nanocrystals with controlled dimensions, surface chemistry, and stabilities. *Sci. Adv.* **2019**, *5*, No. eaax4424.
(61) Hintermayr, V. A.; Lampe, C.; Löw, M.; Roemer, J.; Vanderlinden, W.; Gramlich, M.; Böhm, A. X.; Sattler, C.; Nickel, B.; Lohmüller, T. Polymer nanoreactors shield perovskite nanocrystals from degradation. *Nano Lett.* **2019**, *19*, 4928−4933.
(62) Liu, Y.; Wang, Z.; Liang, S.; Li, Z.; Zhang, M.; Li, H.; Lin, Z. Polar Organic Solvent-Tolerant Perovskite Nanocrystals Permanently

https://doi.org/10.1021/acsenergylett.1c01232
ACS Energy Lett. 2021, 6, 2844−2853

Ligated with Polymer Hairs via Star-like Molecular Bottlebrush Trilobe Nanoreactors. *Nano Lett.* **2019**, *19*, 9019−9028.
(63) Mai, Y.; Eisenberg, A. Self-assembly of block copolymers. *Chem. Soc. Rev.* **2012**, *41*, 5969−5985.
(64) Zhang, T.; Li, G.; Chang, Y.; Wang, X.; Zhang, B.; Mou, H.; Jiang, Y. Full-spectra hyperfluorescence cesium lead halide perovskite nanocrystals obtained by efficient halogen anion exchange using zinc halogenide salts. *CrystEngComm* **2017**, *19*, 1165−1171.
(65) Imran, M.; Ijaz, P.; Baranov, D.; Goldoni, L.; Petralanda, U.; Akkerman, Q.; Abdelhady, A. L.; Prato, M.; Bianchini, P.; Infante, I. Shape-pure, nearly monodispersed $CsPbBr_3$ nanocubes prepared using secondary aliphatic amines. *Nano Lett.* **2018**, *18*, 7822−7831.
(66) Imran, M.; Ijaz, P.; Goldoni, L.; Maggioni, D.; Petralanda, U.; Prato, M.; Almeida, G.; Infante, I.; Manna, L. Simultaneous cationic and anionic ligand exchange for colloidally stable $CsPbBr_3$ nanocrystals. *ACS Energy Lett.* **2019**, *4*, 819−824.
(67) Hu, W.; Wang, Z.; Xiao, Y.; Zhang, S.; Wang, J. Advances in crosslinking strategies of biomedical hydrogels. *Biomater. Sci.* **2019**, *7*, 843−855.
(68) Xu, J.; Liu, X.; Ren, X.; Gao, G. The role of chemical and physical crosslinking in different deformation stages of hybrid hydrogels. *Eur. Polym. J.* **2018**, *100*, 86−95.
(69) De Roo, J.; Ibáñez, M.; Geiregat, P.; Nedelcu, G.; Walravens, W.; Maes, J.; Martins, J. C.; Van Driessche, I.; Kovalenko, M. V.; Hens, Z. Highly dynamic ligand binding and light absorption coefficient of cesium lead bromide perovskite nanocrystals. *ACS Nano* **2016**, *10*, 2071−2081.
(70) Sinatra, L.; Lutfullin, M.; Lentijo-Mozo, S.; Bakr, O. M. 16−5: Late-News Paper: High Flux Stable Perovskite Quantum Dots-Polymer Composite for Down-Converting Applications. *Dig. Tech. Pap. - Soc. Inf. Disp. Int. Symp.* **2020**, *51*, 222−223.
(71) Yang, D.; Li, X.; Zhou, W.; Zhang, S.; Meng, C.; Wu, Y.; Wang, Y.; Zeng, H. $CsPbBr_3$ quantum dots 2.0: Benzenesulfonic acid equivalent ligand awakens complete purification. *Adv. Mater.* **2019**, *31*, 1900767.
(72) Pan, J.; Shang, Y.; Yin, J.; De Bastiani, M.; Peng, W.; Dursun, I.; Sinatra, L.; El-Zohry, A. M.; Hedhili, M. N.; Emwas, A.-H. Bidentate ligand-passivated CsPbI3 perovskite nanocrystals for stable near-unity photoluminescence quantum yield and efficient red light-emitting diodes. *J. Am. Chem. Soc.* **2018**, *140*, 562−565.
(73) Wang, S.; Bi, C.; Portniagin, A.; Yuan, J.; Ning, J.; Xiao, X.; Zhang, X.; Li, Y. Y.; Kershaw, S. V.; Tian, J. $CsPbI_3$/PbSe Heterostructured Nanocrystals for High-Efficiency Solar Cells. *ACS Energy Lett.* **2020**, *5*, 2401−2410.
(74) Imran, M.; Peng, L.; Pianetti, A.; Pinchetti, V.; Ramade, J.; Zito, J.; Di Stasio, F.; Buha, J.; Toso, S.; Song, J.; et al. Halide Perovskite-Lead Chalcohalide Nanocrystal Heterostructures. *J. Am. Chem. Soc.* **2021**, *143*, 1435−1446.

https://doi.org/10.1021/acsenergylett.1c01232
ACS Energy Lett. 2021, 6, 2844−2853

Supporting information for

Switchable Anion Exchange in Polymer-Encapsulated $APbX_3$ Nanocrystals Delivers Stable All-Perovskite White Emitters

Muhammad Imran[a‡*], Binh T. Mai[b‡], Luca Goldoni[c], Matilde Cirignano[d,e], Houman Bahmani Jalali[d], Francesco Di Stasio[d], Teresa Pellegrino[b*], Liberato Manna[a*]

[a] Nanochemistry, Istituto Italiano di Tecnologia, Via Morego 30, 16163 Genova, Italy

[b] Nanomaterials for Biomedical Applications, Istituto Italiano di Tecnologia, Via Morego 30, 16163 Genova, Italy

[c] Analytical Chemistry Lab, Istituto Italiano di Tecnologia, Via Morego 30, 16163 Genova, Italy

[d] Photonic Nanomaterials, Istituto Italiano di Tecnologia, Via Morego 30, 16163 Genova, Italy

[e] Dipartimento di Chimica e Chimica Industriale, Università degli Studi di Genova, Via Dodecaneso 31, 16146 Genova, Italy

Contents

Materials and Methods 2

Extended literature review on polymer encapsulated lead halide pervoskite NCs 5

TEM, DLS, XRD and optical analysis 7

Additional data on switchable anion exchange 12

Ageing tests 13

Detailed NMR analysis 13

Stability tests using various additive molecules 18

Additional data on emitting powders and on the white light emitting layer preparation 23

References 25

Materials and Methods

Chemicals. Poly(acrylic acid)-*block*-poly(styrene) (PAA-*b*-PS) (Mw = 33000 g.mol-1, 20% PAA), Lead bromide ($PbBr_2$,99%), zinc iodide (ZnI_2, 98%) cesium bromide (CsBr, 99%), formamidinium bromide (FABr, 98%) and all additive molecules (Hexan-1-amine, Hexanoic acid, 2-aminoethanethiol, 4-aminobutanoic acid, 5-aminopentanoic acid, (3-aminopropyl)phosphonic acid, 1,4-butandioic acid, 2-amino-3-hydroxypropanoic acid, Pyrrolidine-2-carboxylic acid, 2-amino-3-methylbutanoic acid, 2-amino-5-(diaminomethylideneamino)pentanoic, 2-Aminopentanedioic acid, -2-Amino-3-sulfhydrylpropanoic acid, 2-Amino-3-(1H-imidazol-4-yl)propanoic acid, 2-aminotertphthalic acid), poly(vinyl alcohol) (PVA, Mw 85,000-124,000), Oleylamine (OLAM, 98%), Polystyrene (PS, Mw 35,000) and Iodine (I_2, 99.99%) were purchased from Sigma-Aldrich. Didodecyldimethylammonium Chloride (DDACl, 98%) was purchased from TCI. All the chemicals were used as received. All the solvents (hexane, toluene, dimethylformamide (DMF) were also purchased from Sigma-Aldrich and used without further purification.

Synthesis of Polymer-encapsulated $APbBr_3$ Nanocrystals. Metal bromide salts (CsBr, FABr and $PbBr_2$: 10 mM each) additive molecules (for example 5-aminopentanoic acid, APAc, the concentration of the additive molecules was kept the same - 17 mM - in all experiments) and polymer (PAA-*b*-PS, 110 mg/mL) were first separately dissolved in DMF. Then, a mixture of ABr (100 µL), $PbBr_2$ (100 µL), APAc (4 µL) and PAA-*b*-PS (75 µL) precursor's solutions in DMF was injected dropwise into a 20 mL vial containing toluene (8 mL) under vigorous stirring at room temperature in air (see figure 1). The color of the solution turned green immediately, indicating the formation of perovskite NCs. The mixed cation $Cs_{0.5}FA_{0.5}PbBr_3$ NCs were prepared by using 1:1 molar ratios of CsBr and FABr precursors directly in the synthesis. After about 20 seconds, the reaction was quenched by adding excess of hexane and the NCs were collected by centrifugation. Then, the supernatant was discarded and the precipitate was re-dispersed in toluene followed by another round of centrifugation and re-dispersion. The toluene dispersion of the NCs was centrifuged once again (at 6000 rpm for 10 min), the colloidally unstable fraction was discarded and the supernatant was collected for further uses.

Halide exchange reactions: All the reactions were performed under ambient conditions. To tune the emission color from green to blue, green emitting polymer-encapsulated $CsPbBr_3$ NCs dispersions in toluene were mixed with a DDACl solution (pre-dissolved in toluene, 25 mM concentration) under continuous stirring. To prepare the red emitting NCs, oleylammonium iodide (OLAM-I) (prepared separately by reacting molecular iodine with oleylamine, 0.4 M I^-)[1] was used instead. We observed that the oleylammonium iodide is weakly soluble in methanol. To further verify the switchable behavior of the iodide exchange reaction in our polymer encapsulated NCs, we choose ZnI_2 salt as a source of iodine ions. Notably, ZnI_2 is high soluble in methanol and has been used for halide exchange reactions in toluene dispersions of halide exchange reactions in toluene dispersions of perovskite NCs.[2] Briefly, ZnI_2 was directly added in toluene and methanol dispersions of PAA-*b*-PS encapsulated green emitting NCs. In the case of the methanol dispersion, the color of the starting NCs was preserved, despite the addition of a large excess of ZnI_2. On the other hand, in the toluene dispersion of the NCs, the color of the sample quickly changed from green to red upon addition of ZnI_2.

Preparation of the white emitting powder. The PAA-*b*-PS encapsulated $Cs_{0.5}FA_{0.5}PbBr_3$ NCs were prepared first using aminobutyric acid as an additive molecule and subsequently subjected to halide exchanged reactions for the preparation of other compositions. Briefly, the toluene dispersion of PAA-*b*-PS-$Cs_{0.5}FA_{0.5}PbBr_3$ NCs were treated with DDACl and OLAM-I to obtain blue and red emitting samples respectively. Once the desired emission color for the blue (480 nm) and red (625 nm) emitting samples was achieved, hexane in excess was added to the NCs dispersion (with volume ratio of 1:5, toluene to hexane) and the resulting mixture was centrifuged at 6000 rpm for 5 minutes. Thereafter, the supernatant was discarded and the precipitate was re dispersed in toluene. Then, PAA-*b*-PS-$Cs_{0.5}FA_{0.5}PbX_3$ NCs with desired emission color in toluene dispersion were separately mixed with poly(methyl methacrylate) pre-dissolved in toluene (50 mg/mL). Finally, the polymer shell of PAA-b-PS micelles

encapsulating the NCs was "closed" by adding a mixture of methanol and hexane (with a volume ratio of 1:5) to the toluene dispersion of the PAA-*b*-PS-$Cs_{0.5}FA_{0.5}PbX_3$ (X=Br and Br/Cl) NCs, while only hexane was added in case of PAA-*b*-PS-$Cs_{0.5}FA_{0.5}Pb(BrI)_3$ NCs. The resulting mixture was centrifuged again at 6000 rpm for 5 minutes and the supernatant was discarded. The precipitate was dried in a vacuum oven at 40 °C overnight. The obtained powders were individually ground with a ball mill (SPEX SamplePrep 8000M MIXER/MILL). The green and blue emitting samples were ball milled for 5 minutes, while red emitting sample for 2 minutes. The obtained fine powders were then mixed in an appropriate ratio to get a white emitting NCs powder.

White LED fabrication. The white emitting samples were prepared by mixing red, green and blue emitting powders of PAA-*b*-PS encapsulated $Cs_{0.5}FA_{0.5}PbX_3$ (X=Br and Br/Cl) NCs in an approximate ratio of 1:2:3 in weight (green:blue:red) was added to the water solution of polyvinyl alcohol (PVA, 210 mg/mL). Thereafter, the sample was drop-cast on a quartz substrate and subsequently dried for 15 min at 65°C. Then, white emitting film was placed on a 365 nm LED (maximum power of 1 W) which was used for excitation. A 425 nm long pass filter (Thorlabs) was then placed onto the PVA film to remove the UV excitation light, see the device structure in Figure S23.

Morphological characterization. TEM images of the NC samples were acquired with a JEOL-1100 transmission electron microscope operating at an acceleration voltage of 100 kV. Samples were prepared by drop casting diluted solutions of NCs onto carbon film-coated 200 mesh copper grids.

Structural characterization. Structural analysis was performed on a PANanalytical Empyrean X-ray diffractometer, equipped with a 1.8 kW CuKα ceramic X-ray tube, operating at 45 kV and 40 mA, and a PIXcel3D 2×2 area detector. A colloidal dispersion of corresponding NCs was drop-cast on a zero-diffraction silicon substrate. All the diffraction patterns reported in this work were collected at room temperature under ambient conditions using parallel beam geometry and symmetric reflection mode. Post-acquisition XRPD data analysis was carried out using the HighScore 4.1 software from PANalytical.

Spectroscopic measurements. Optical absorption spectra were recorded using a Varian Cary 300 UV-VIS absorption spectrophotometer. The PL spectra were measured on a Varian Cary Eclipse spectrophotometer using an excitation wavelength (λ_{ex}) of 350 nm for all the samples. Samples were prepared by diluting NC solutions in toluene, in quartz cuvettes with a path length of 1 cm. Absolute Photoluminescence quantum yields of NC samples were measured using an Edinburgh FLS900 fluorescence spectrometer equipped with a Xenon lamp, a monochromator for steady-state PL excitation, and a time-correlated single photon counting unit coupled with a pulsed laser diode (λ_{ex} = 405 nm, pulse width = 50 ps) for time-resolved PL. The PLQY was measured using a calibrated integrating sphere (λ_{ex} = 350 nm for all samples). For the PLQY measurements, all the NC dispersions were diluted to an optical density of 0.1 ±0.02 at the corresponding excitation wavelength in order to minimize the amount of fluorophore being reabsorbed.

Sample preparation for high flux irradiation experiments. PAA-*b*-PS encapsulated $CsPbBr_3$, $Cs_{0.5}FA_{0.5}PbBr_3$ and $FAPbBr_3$ NCs samples were prepared using AVAc as an additive molecule. The "reference" $CsPbBr_3$ NCs were prepared using hot injection method developed by Protesescu et al.[3] The toluene dispersions of all samples including the reference sample with the concentration 10-12 mg/mL were mixed with a polystyrene solution (30 mg/mL in toluene). The resulting mixture was precipitated by adding 12 mL of hexane, followed by overnight drying in vacuum oven at 40 °C. Then, the powder was grounded by using a mortar and pestle set and was then placed inside a glass cell.

Laser irritation stability tests. Stability tests were carried out using a continuous wave laser diode for excitation (λex = 445 nm, Oxxius LBX-445-650-HPE-PP, max power 715 mW) coupled with an iris to reduce the circular excitation spot to a diameter of 1mm (spot size was determined with Thorlabs BP209-VIS/M beam profiler). The excitation power was measured after the iris using a Thorlabs PM100D Digital Optical Power meter interfaced with a Thorlabs S121C photodiode. The emission was monitored via a collimator/optical fiber/filter

holder/optical fiber assembly coupled with an Ocean Optics HR4000 spectrometer. The collection optics was placed at 45° with the respect to the excitation beam and a long pass filter (λcut-off = 450 nm, Thorlabs FEL0450) was placed in the fiber coupled filter holder. The emission was collected every 60 seconds using the Ocean View software.

DLS measurements. The hydrodynamic sizes of the particles were measured by Dynamic Light Scattering (DLS) using a Malvern Instruments Zetasizernano series instrument. Prior to each reading, the sample was left for 1 min to equilibrate and triplicate measurements were done for each sample.

NMR measurements. NMR experiments were performed at 298 K on a Bruker AvanceIII 600 MHz spectrometer equipped with 5 mm QCI cryoprobe with z shielded pulsed-field gradient coil. The free polymer sample was prepared by dissolving 8.25 mg of PAA-b-PS powder in 1mL of DMF-d7. The PAA-b-PS micelles sample was prepared by dissolving the same amount of polymer into DMF followed by drop-wise addition of the polymer solution into toluene to induce the micelle formation. Thereafter, the micelles were collected by adding hexane in access to the crude solution followed by centrifugation at 5000 rpm for 5 minutes. The supernatant was discarded and the dried precipitate was redispersed in d-8 toluene. For the liquid state NMR measurements, the samples were transferred into 5 mm disposable NMR tubes (Bruker). Before each acquisition, automatic matching and tuning (both on 1H and 13C) and homogeneity were adjusted.

In the *^{1}H-NMR experiments*, 128 transients were accumulated after having applied a 90 degree of flip angle excitation pulse, with relaxation delay of 30 s, over a spectral width of 20.55 ppm (offset at 10 ppm).

In the *^{13}C NMR spectra* (inverse gated ^{1}H decoupling), 10752 transients were collected after a 30-degree pulse, with 32768 of digit points, an interpulses delay of 3.5 s, over a spectral width of 240.1 ppm (offset at 100 ppm).

An apodization exponential function equivalent to 0.1 and 15 Hz were applied to the ^{1}H and ^{13}C FIDs respectively, before the Fourier transform.

The *^{1}H-^{13}C HSQC* (multiplicity edited Heteronuclear Single Quantum Coherence, with the selection of CH_2 and CH/CH_3 in opposite phases, graphically represented in blue and red respectively) was performed with 32 FIDs, 2048 data points, 256 increments, over a spectral width of 15.02 ppm for ^{1}H and 165.7 ppm for ^{13}C (transmitter frequency offsets at 7.45 and 74.6 ppm, respectively).

The *^{1}H-^{13}C HMBC* (Heteronuclear Multiple Bond Correlation) was acquired with 128 FIDs, 2048 data points, 128 increments, over spectral width of 15.02 ppm for ^{1}H and 222.1 ppm for ^{13}C (transmitter frequency offsets at 7.48 and 99.8 ppm, respectively).

All spectra were referred to the not deuterated residual solvent peaks, at 7.09 and 129.2 ppm (toluene-d_7), and at 8.03 and 163.2 ppm (DMF-d_6), for ^{1}H and ^{13}C, respectively.

Extended literature review on polymer encapsulated lead halide pervoskite NCs

Various studies have studies have shown that embedding perovskite NCs in different polymeric matrices significantly improves their stability. Among those, encapsulation of individual MHP NCs is most the appealing and gain signifincat attention of the scientific community in recent past. Hou et al. back in 2017 used polystyrene-*block*-poly-2-vinylpyridine (PS-*b*-P2VP) micelles to prepare PS-*b*-P2VP coated $CsPbX_3$ NCs.[4] This strategy was later adopted by Lohmuller et al. to prepare the PS-*b*-P2VP coated $MAPbX_3$ NCs.[5] In both studies, the nanoreactors were prepared initially by dissolving P4VP-*b*-PS in toluene, followed by the addition of the corresponding halide salts (such as CsX, MAX and PbX_2) sequentially. Given a lower solubility of metals salts in toluene, Hou et al. noted that the mixture of nanoreactors and metal halide salts ($PbBr_2$) needed to be kept under continuous stirring for at least two weeks to achieve 0.1 mg/mL loading of the corresponding salt. This however makes the procedure reported by Hou et al. and Lohmuller et al. et al. not only time consuming but also not much useful, as it leads to a very low yield of the final material. In terms of stability, Hou et al. reported that PS-*b*-P2VP capped $CsPbBr_3$ NCs completely lost their PL in a mixture of methanol and toluene (with a volume ratio of 10 to 1) within 2 minutes upon dispersion (see Figure 3 of their manuscript). Lohmuller et al., on the other hand, reported that the PS-*b*-P2VP encapsulated $MAPbBr_3$ NCs have improved stability against moisture, water and weak UV irradiation. The high stability of perovskite NCs against a short chain alcohol such as methanol remains an unachieved goal so far. This is most likely due to the fact that methanol is less hydrophilic and has a lower surface tension compared to water, hence it will have higher tendency to penetrate through the PS protective layer which consequently makes it more detrimental for the perovskite NCs compared even to water. This was indeed observed experimentally on the PS-*b*-P2VP capped perovskite NCs prepared by Hou et al.

Lin et al. recently used a multiarm star-like amphiphilic triblock copolymer, namely poly(4-vinylpyridine)-*block*-poly(tert-butyl acrylate)-*block*-polystyrene (denoted P4VP-*b*-PtBA-*b*-PS), to encapsulate perovskite NCs.[6] In that study, a three-step synthesis was used to prepare $MAPbX_3$ NCs coated with a SiO_2 middle layer and PS as the outer shell. Due to the unique molecular structure of the polymer, the micelles are made of 21 chains of triblock copolymer (1st segment of P4VP for $MAPbX_3$ nucleation, 1 middle segment of PtBA to yield PAA upon the thermolysis to bestow the capability to grow a silica shell and last outer segment of PS to improve the stability) linked together through a knot at the end of the P4VP block. Although this approach is elegant, the micelles made of multi-arm star-like amphiphilic triblock copolymers have a rather low density of PS shell (21 chains per micelles) in comparison to the conventional self-assembled micelles made of linear diblock copolymers. This in turn provides a low barrier against a polar environment. Indeed, the authors observed that the growth of the SiO_2 shell between the PS layer and the $MAPbX_3$ layer is crucial to achieve a good stability against water. Also in that case, the stability against short chain alcohols was not addressed. Similarly, in another study reported by the same group, Liu et al. used a star-like molecular bottlebrush trilobe, poly(2-hydroxyethyl methacrylate)-*graft*-(poly(acrylic acid)-*block*-partially cross-linked polystyrene (denoted PHEMA-*g*-(PAA-*b*-cPS)) to act as a polymeric nanoreactor.[7] The authors reported that the $CsPbBr_3$ is formed within the PAA block while PS block acts as the protective layer. Owing to its trilobe structure, such polymer will not be able to self-assemble to form a classical micellar structure due to the constraint of the chain. This, in turn, will create some defects in the protective PS layer (not uniform hairy shell), thus allowing the penetration of solvents through the PS shell. The authors indeed reported that polymer coated NCs could withstand 20-30% volume of methanol for less than 20 days. Further increase in the methanol volume (40 % or higher) resulted in a complete loss of PL instantly upon dispersion.

Table S1: Comparison of key features of the present work with previous reports

	Material type ($APBX_3$)	Polymer composition	Synthesis conditions	Switchable anion exchange reaction	Stability against polar solvents (Colloidal)			High flux irradiation stability	Stable multicolor emitters	Fully perovskite based white LED
					Water	Ethanol	Methanol			
This study	Cs, FA	PAA-b-PS, linear	single step, RT	Yes	Complete retention of PLafter 23 days (100% water)	20% of PL lost after 23 days (100% EtOH))	50% of PL lost after 23 days (100% MeOH)	Yes (3.2 W/cm^2)	Yes	Yes
Ref. [4]	Cs	P4VP-b-PS, linear	2 step, RT	No	Complete loss of PL was observe after 25 hours of dispersion	Complete loss of PL after 40 days (90% EtOH in toluene)	Complete loss of PL upon dispersion (81% methanol in toluene)	N.A.	N.A.	NO
Ref. [6]	MA	P4VP-b-PAA-b-PS Multi-arm star like (21 arms per micelles). The growth of SiO2 layer in PAA block is crucial for the stability	3 step, HT	No	Yes (in film)	N.A.	N.A.	N.A	Yes	NO
Ref. [5]	MA	P4VP-b-PS, linear	2 step, RT	No	Yes (in film)	N.A.	N.A.	N.A.	Yes	NO
Ref. [7]	Cs	PAA-b-PS-grafted PHEMA, trilobe	single step, RT	No	Nearly stable against10 % water	N.A	Not stable in complete methanol dispersion	N.A	N.A	NO

TEM, DLS, XRD and optical analysis

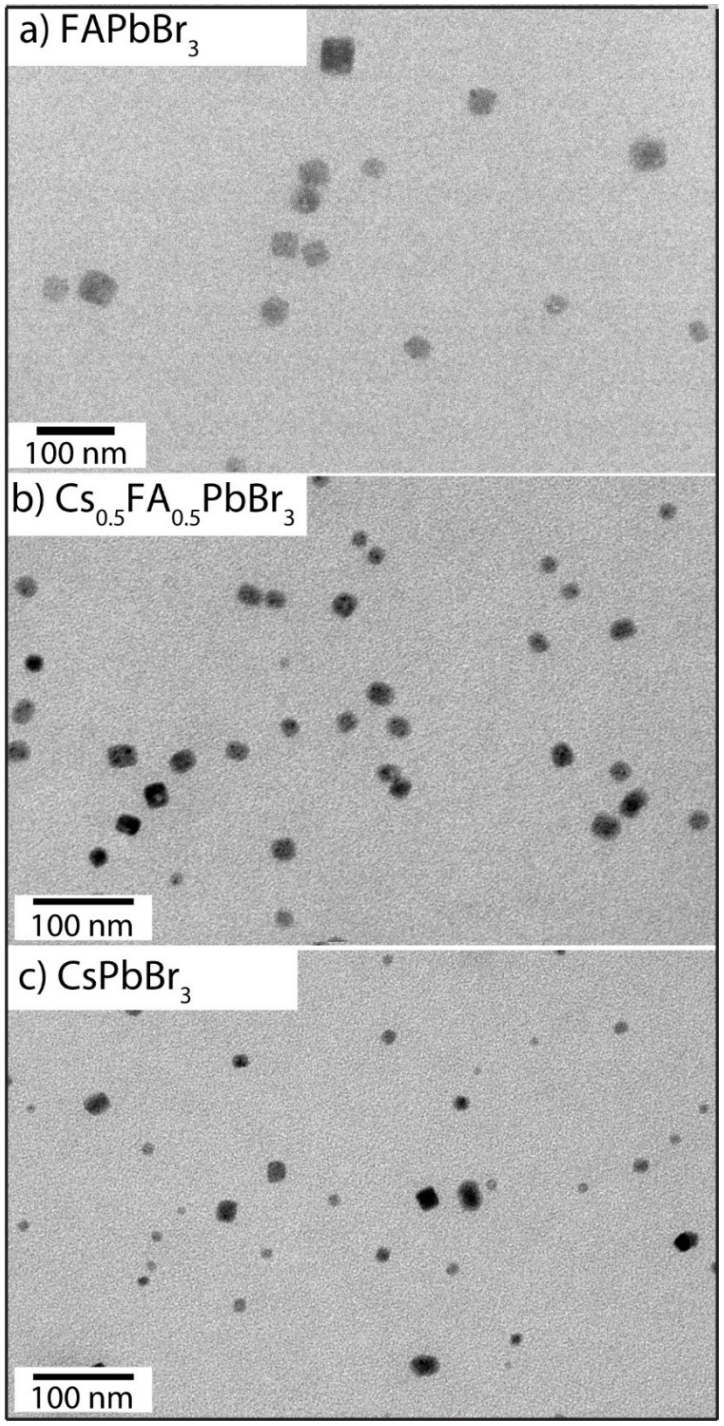

Figure S1. TEM images of PAA-*b*-PS encapsulated $CsPbBr_3$, $Cs_{0.5}FA_{0.5}PbBr_3$ and $FAPbBr_3$ NCs samples deposited from toluene dispersions.

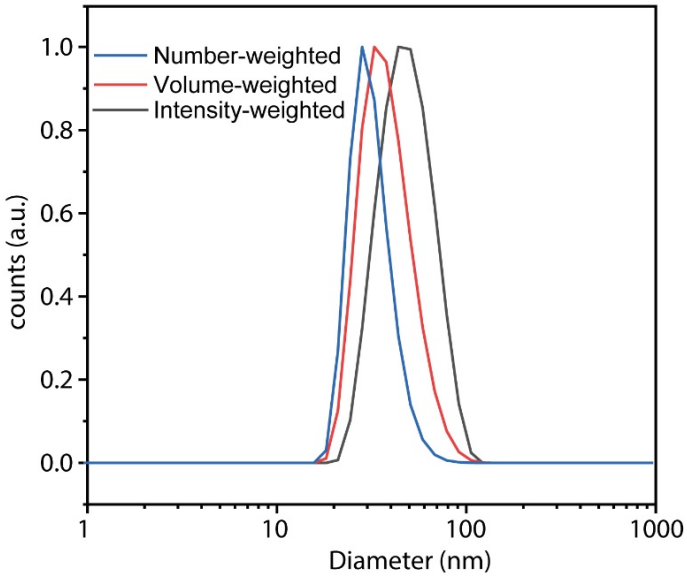

Figure S2. Dynamic light scattering (DLS) traces of PAA-*b*-PS dispersions in toluene.

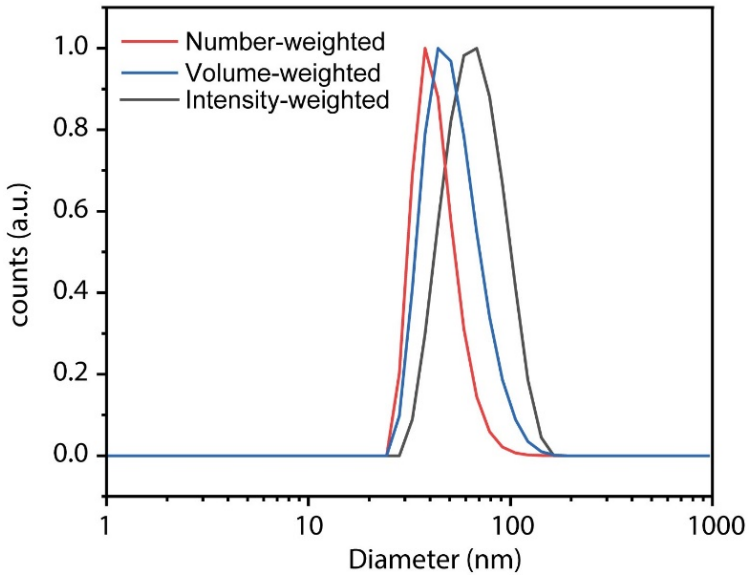

Figure S3. DLS traces of PAA-*b*-PS encapsulated $CsPbBr_3$ NCs dispersions in toluene.

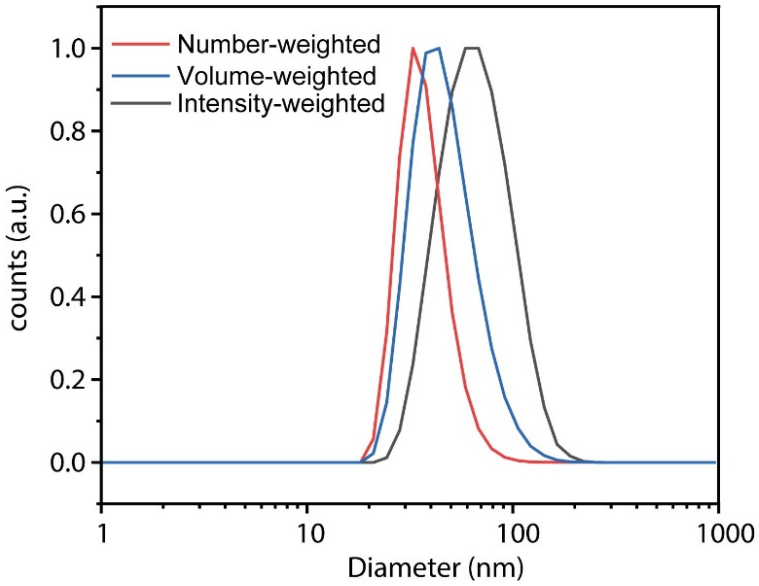

Figure S4 DLS traces of PAA-*b*-PS encapsulated $Cs_{0.5}FA_{0.5}PbBr_3$ NCs dispersions in toluene.

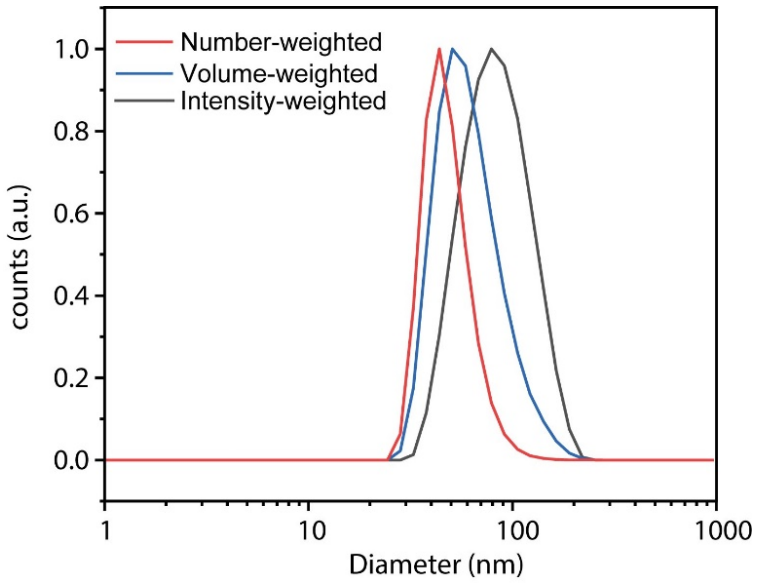

Figure S5. DLS traces of PAA-*b*-PS encapsulated $FAPbBr_3$ NCs dispersions in toluene.

Table S2. Hydrodynamic diameters (d_H) weighted by intensity, volume and number along with polydispersity index (PDI) of free micelles and PAA-*b*-PS encapsulated $CsPbBr_3$, $Cs_{0.5}FA_{0.5}PbBr_3$, $FAPbBr_3$ NCs.

Sample	d_H (intensity) (nm)	d_H (volume) (nm)	d_H (number) (nm)	PDI
PAA-*b*-PS free micelles	50 ± 1	39 ± 1	32 ± 1	0.10 ± 0.01
PAA-*b*-PS-$CsPbBr_3$	69 ± 1	53 ± 1	43 ± 1	0.08 ± 0.01
PAA-*b*-PS-$Cs_{0.5}FA_{0.5}PbBr_3$	69 ± 3	49 ± 2	38 ± 3	0.13 ± 0.03
PAA-*b*-PS-$FAPbBr_3$	86 ± 1	65 ± 1	49 ± 1	0.06 ± 0.01

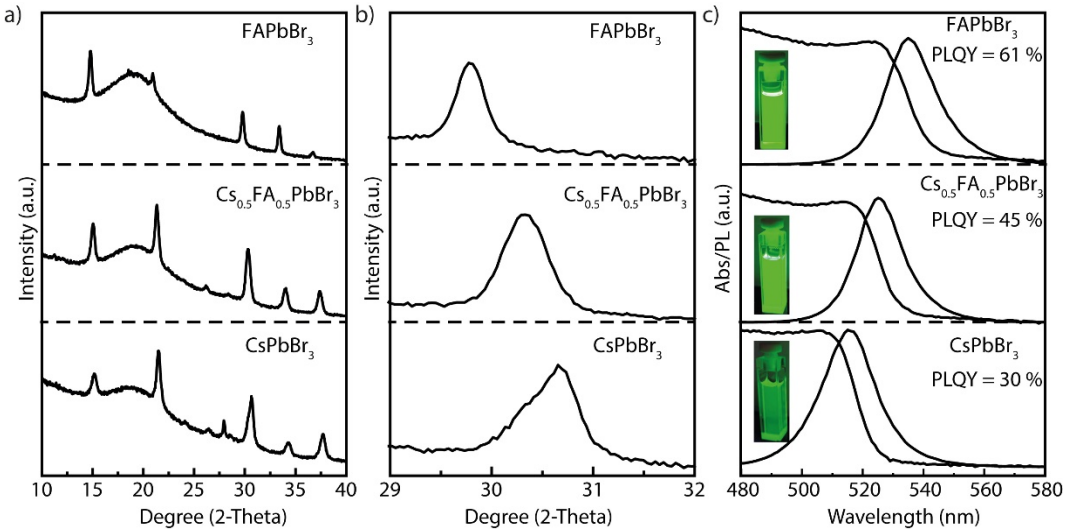

Figure S6. (a) XRD patterns of PAA-*b*-PS encapsulated $CsPbBr_3$, $Cs_{0.5}FA_{0.5}PbBr_3$ and $FAPbBr_3$ NCs. The small hump at 18° (2θ) present in all three samples can be ascribed to the presence of the polymer. (b) Magnified view of the XRD patterns reported in (a), in the 29-32° 2θ range (b). (c) Optical absorption and PL spectra recorded on toluene dispersions of the various samples, along with photos of the same samples recorded under the irradiation of a UV lamp. The extended range of absorption and PL spectra of these sample is reported in Figure S7.

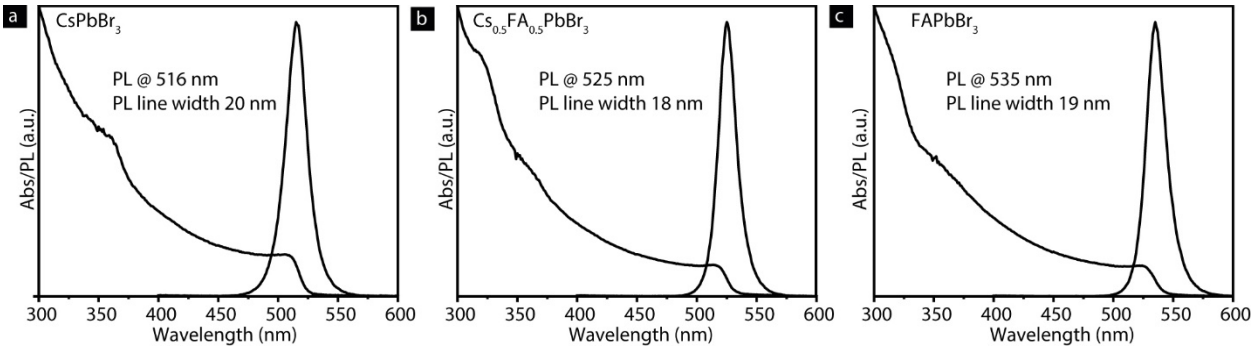

Figure S7. Optical absorption and PL spectra of PAA-b-PS encapsulated (a) $CsPbBr_3$, (b) $Cs_{0.5}FA_{0.5}PbBr_3$ and (c) $FAPbBr_3$ NCs dispersions in toluene.

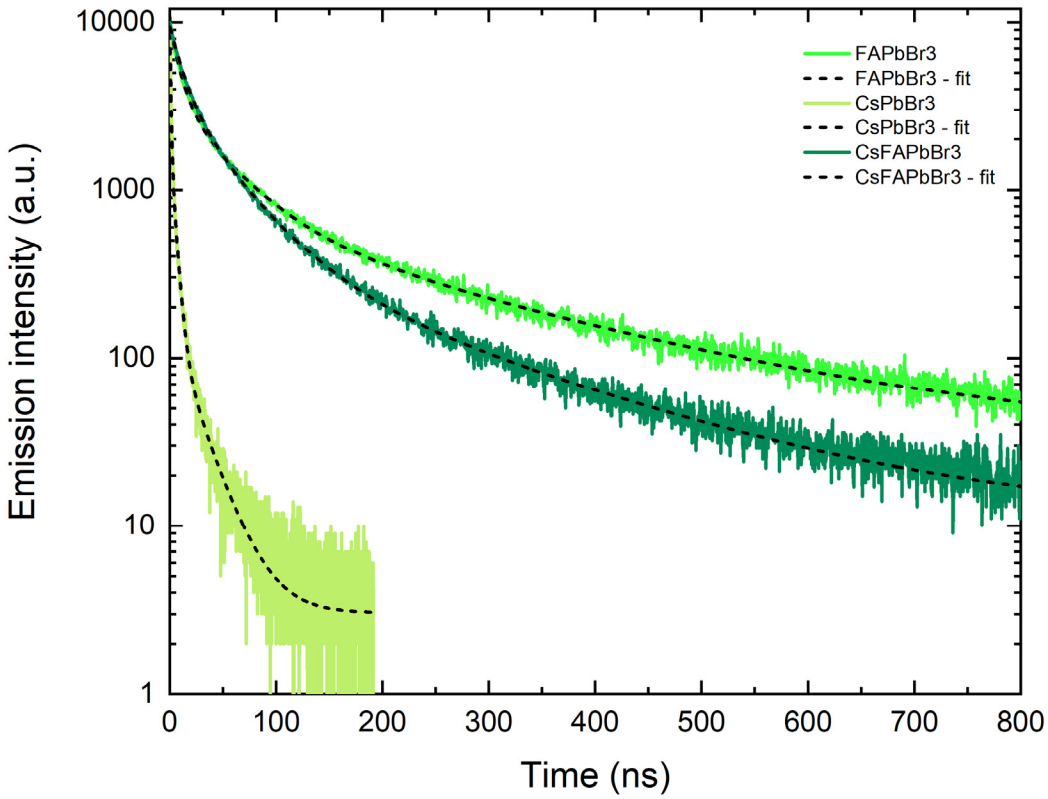

Figure S8. PL lifetimes of the PAA-b-PS encapsulated NCs reported in Figure S1 and S6. The measurements were performed in toluene dispersions. The PL decays were fitted with the following expression: Fit = A + B1*exp(-t/T1) + B2*exp(-t/T2) + B3*exp(-t/T3) (values reported in Table S1).

Table S2: PL lifetime data extracted from the fittings of plots reported in Figure S8 of PAA-b-PS encapsulated NCs. The reported amplitude and intensity weighted average lifetime were calculated using the following expressions:

Intensity Average lifetime = (B1*(T1)^2+B2*(T2)^2+B3*(T3)^2)/(B1*T1+B2*T2+B3*T3), Amplitude Average lifetime = (B1*T1+B2*T2+B3*T3)/(B1+B2+B3).

Sample name	Lifetime (ns)		Intensity (a.u.)	Rel. Contribution (%)	Intensity weighted Average lifetime (ns)	Amplitude weighted Average lifetime (ns)
$CsPbBr_3$						
T1	0.8	**B1**	9884	41.58	6	1.64
T2	4.2	**B2**	1896	41.21		
T3	22.8	**B3**	147	17.21		
$Cs_{0.5}FA_{0.5}PbBr_3$						
T1	11.8	**B1**	5582	21.24	75.9	32.2
T2	44.5	**B2**	3547	50.99		
T3	183	**B3**	468	27.77		
$FAPbBr_3$						
T1	9.1	**B1**	6126	15.86	124	35.9
T2	46	B2	2944	38.63		
T3	231	B3	690	45.51		

Additional data on switchable anion exchange

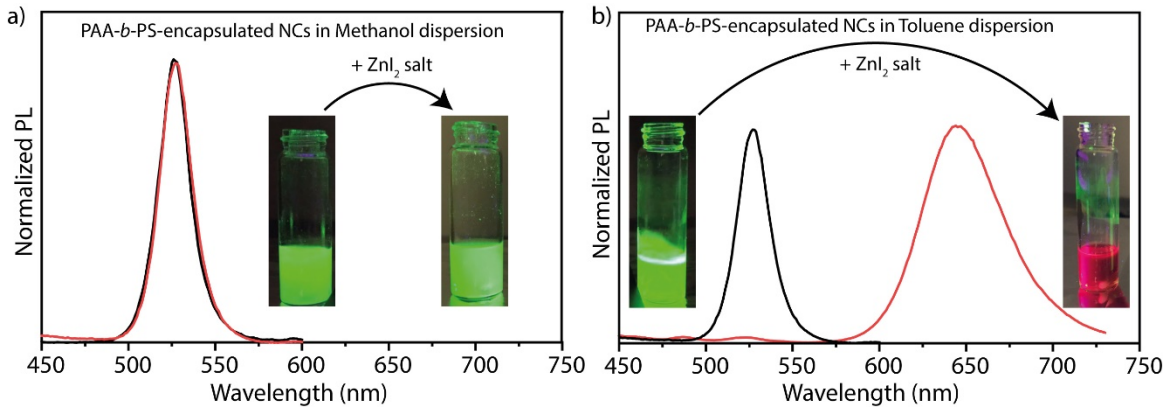

Figure S9. Switchable halide exchange reactions using zinc iodide. PL spectra of the initial $CsPbBr_3$ NCs sample dispersed in toluene (black curve) and the corresponding samples upon the addition of zinc iodide (red curve) in methanol dispersion (a) and toluene dispersion (b), respectively. The inset in both panels shows the photographs of NCs dispersions recorded under UV-lamp irradiation before and after halide exchange reactions.

Ageing tests

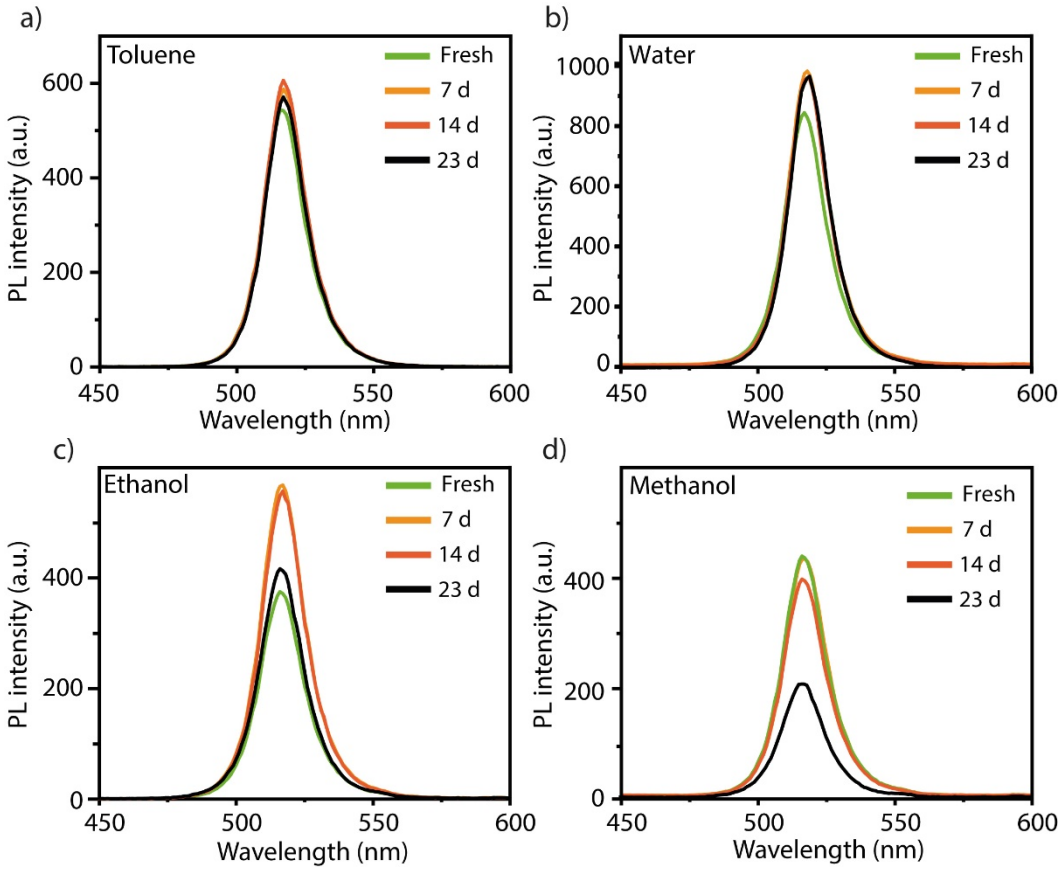

Figure S10: Stability of PAA-b-PS encapsulated $CsPbBr_3$ NCs over ageing in different solvents. (a) toluene, (b) water, (c) ethanol, (d) methanol. Samples were stored in cuvettes under ambient air and PL spectra were recorded over the period of 23 days.

Detailed NMR analysis

We performed detailed liquid state nuclear magnetic resonance (NMR) spectroscopy to confirm that the micelles have an outer shell of PS and an inner core of PAA. The NMR measurements include ^{1}H, ^{13}C, 2D ^{1}H-^{13}C, Heteronuclear Single Quantum Coherence (HSQC) and ^{1}H-^{13}C Heteronuclear Multiple Bond Correlation (HMBC). The experiments were performed on the starting free PAA-*b*-PS, empty PAA-*b*-PS micelles and PAA-*b*-PS encapsulated NCs. The free polymer sample was prepared by dissolving 8.25 mg of PAA-*b*-PS powder in 1mL of DMF-d7. The PAA-*b*-PS micelles sample was prepared by dissolving the same amount of polymer into DMF followed by drop-wise addition of the polymer solution into toluene to induce the micelle formation. Thereafter, the micelles were collected by adding hexane in excess to the crude solution, followed by centrifugation at 5000 rpm for 5 minutes. The supernatant was discarded and the dried precipitate was redispersed in d-8 toluene. The PAA-*b*-PS encapsulated NCs sample was prepared under the same conditions as those used for the empty micelles, but with the addition of metal

bromides (CsBr and $PbBr_2$) and the solution containing the additive molecules. For NMR measurements, the samples were transferred into 5 mm disposable NMR tubes (Bruker).

We initially performed the ^1H, ^{13}C, 2D ^1H-^{13}C, HSQC and ^1H-^{13}C HMBC NMR analysis on the starting free PAA-*b*-PS in DMF-d_7 as a solvent, see the results in Figure 3 c, d and Figure S11. DMF is a non-selective solvent for the polymer, therefore both the PAA and PS components of the polymer should be detectable through ^1H and ^{13}C NMR. The ^1H NMR analysis clearly evidenced the resonances corresponding to OH (1) of the carboxylic acid group (δ 12.66 ppm) and the CH (3) in position α to the CO group (δ 2.49 ppm) of the PAA component, along with the aromatic region (δ from 6.38 to 7.69 ppm) of the PS part of the polymer. Analogously, the CO (2) group (δ 176.4 ppm) of the PAA block, as well as the aromatic (5-8) signals (δ from 147.4 to 125.3 ppm) of the PS moiety are detectable in the ^{13}C spectrum, see Figure 3d of the main text. Interestingly, the 2D ^1H- ^{13}C HSQC spectra, along with the ^1H-^{13}C HMBC cross correlations, which unambiguously confirm the cross correlations between the peaks (3) and (4) and the CO group (2) of the acidic function of the PAA moiety, enabled us to provide a complete assignment of the ^1H and ^{13}C peaks. Then, we ran the same analysis on PAA-*b*-PS micelles made from same polymer (the preparation of both samples is described in the previous paragraph) in toluene d-8. The results of ^1H, ^{13}C, 2D ^1H-^{13}C, HSQC and ^1H-^{13}C HMBC NMR are reported in Figure 3 c, d top panels and Figure S12. The characteristic signals the carboxylic proton COOH (1, δ from 13.0 to 11.0 ppm) and of the CH proton (3) in position α to the CO group (δ ~ 2.5 ppm), which are distinguishable footprints of the PAA block, are not detectable. This is in line with the ^{13}C spectrum, in which the signal of C=O (δ from 180.0 to 170.0 ppm) is not noticeable (Figure 3d, top panel). These evidences indicate that the PAA block has a very poor mobility in toluene (it remains inaccessible to the solvent) and the only contribution to the high resolution NMR peaks is due to the PS moiety. We further recorded the ^1H NMR spectrum of the PAA-*b*-PS encapsulated NCs in toluene-d_8 and compared it with the ^1H NMR spectrum of the empty micelles (see Figure S13). The spectrum of the empty PAA-b-PS micelles has peak profiles and signal widths at half height that are identical to those of the micelles with the NCs inside, thereby confirming the similar structure of the polymer micelles in both cases. These measurements overall confirm that PAA forms the core of the micelles encapsulating the perovskite NCs while PS forms the outer shell. Overall, our NMR analysis verifies the structural conformation of the polymer, which consists of PAA as a rigid core and a PS outer shell, the latter exposed to the solvent thus more flexible.

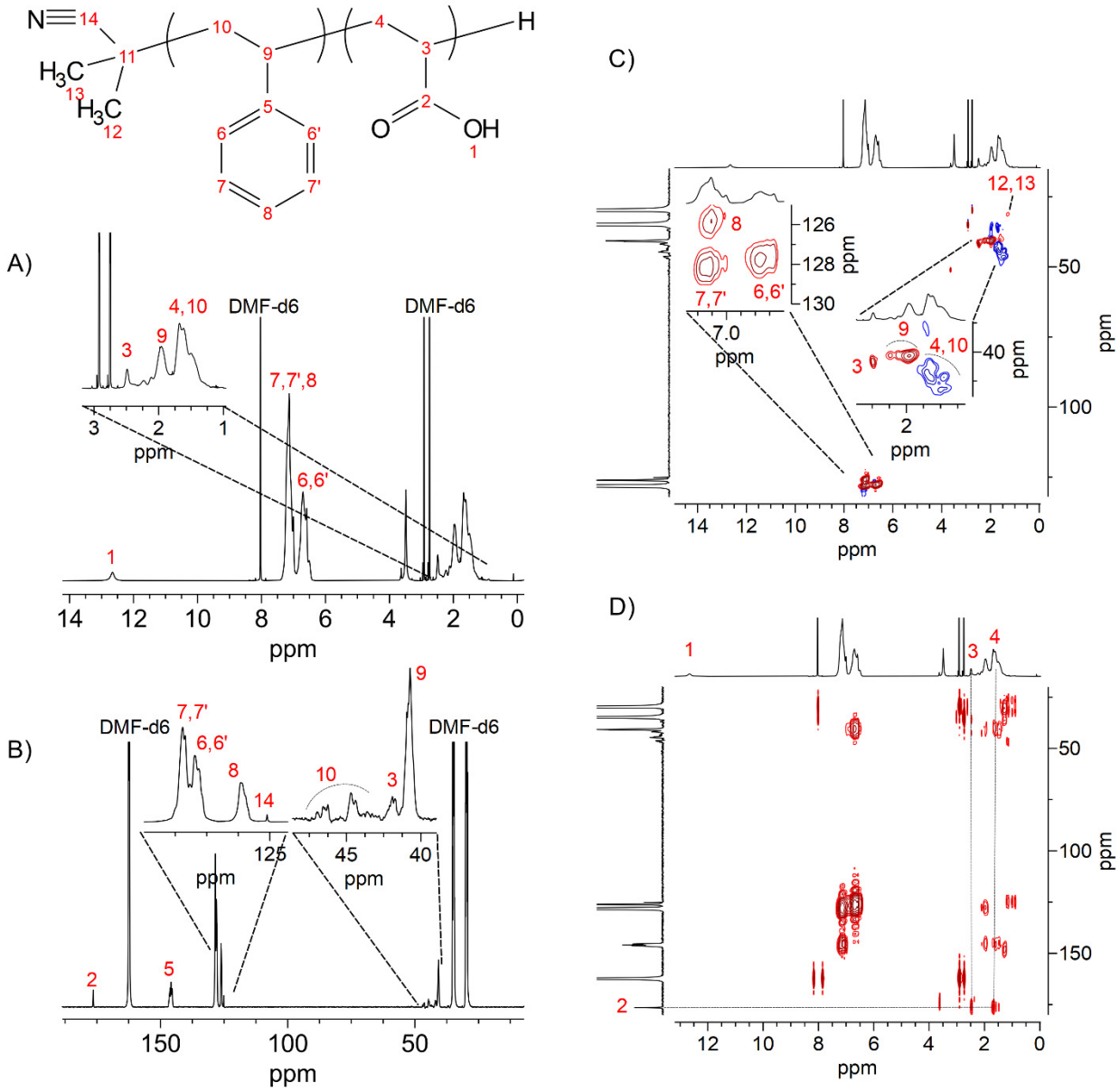

Figure S11. ^{1}H (A), ^{13}C (B), ^{1}H-^{13}C HSQC (C) and ^{1}H-^{13}C HMBC (D) NMR spectra of the free PAA-b-PS polymer dissolved in DMF-d$_7$ The spectra reveal all the characteristic ^{1}H and ^{13}C peaks of the PAA-b-PS structure, along with their peak assignments, and ^{1}H-^{13}C HMBC cross correlations. HMBC allows the possibility to identify the correlation between ^{1}H and distant ^{13}C (1-2 bonds). Here, HMBC confirm unambiguously the assignment of peak 3 of PAA moiety, through the HMBC cross correlations (dashed lines in the figure S11 D) between the signals 3 and 4, and the signal 2, whose ^{13}C resonance (at 176.4 ppm) is uniquely attributed to a C=O group of the acidic function of PAA moiety.

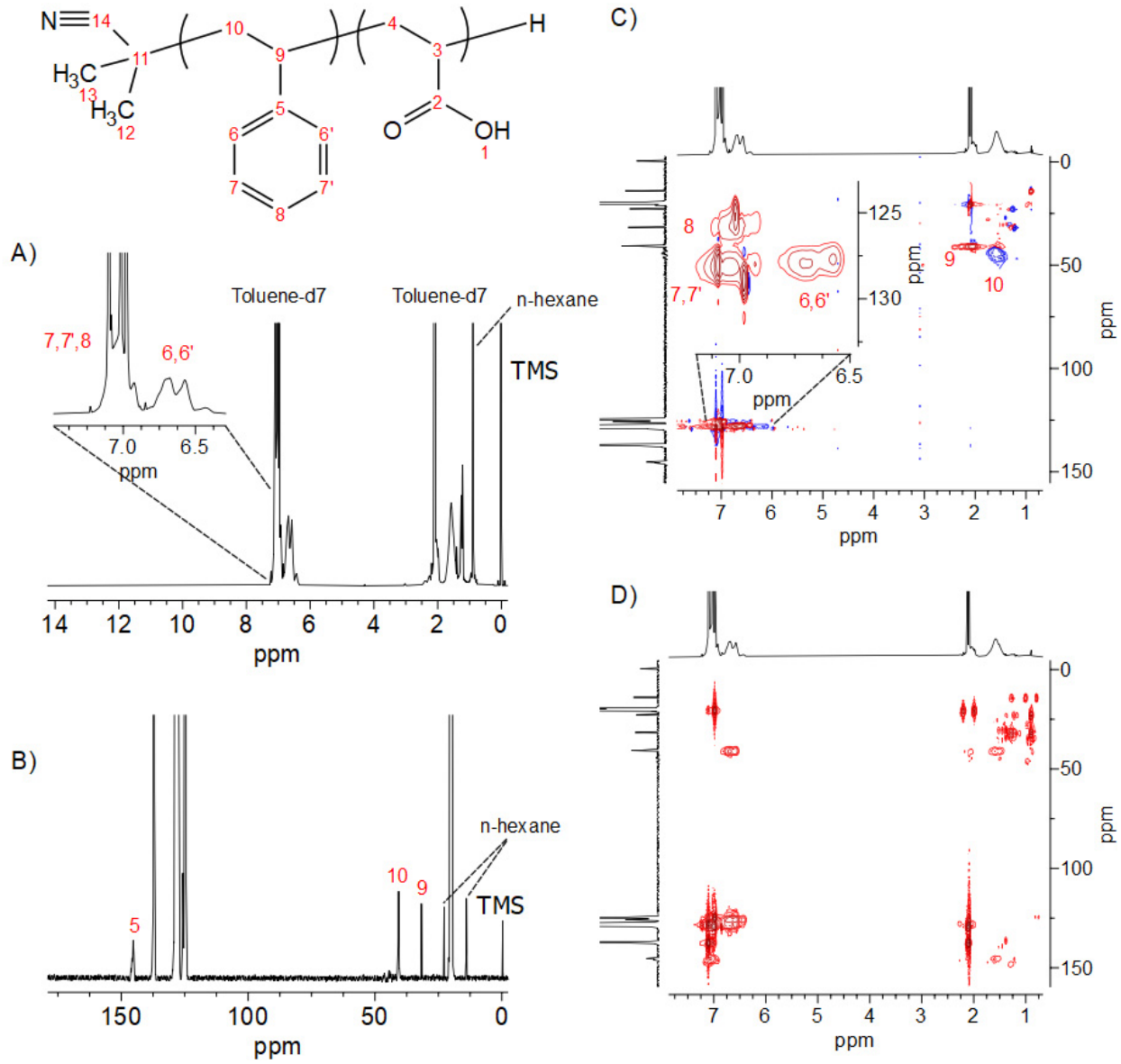

Figure S12: ^{1}H (A),^{13}C (B), ^{1}H-^{13}C HSQC (C) and ^{1}H-^{13}C HMBC (D) NMR spectra of empty PAA-b-PS micelles dispersed in toluene-d_8. The spectra reveal all the characteristic ^{1}H and ^{13}C peaks of the PS structure along with their unambiguous peak assignments and ^{1}H-^{13}C correlation (2D NMR). In toluene-d_8, the ^{1}H and ^{13}C signals of PAA block are missing. These evidences indicate that PAA moiety has a poor mobility in toluene, which is consistent with a rigid core conformation.

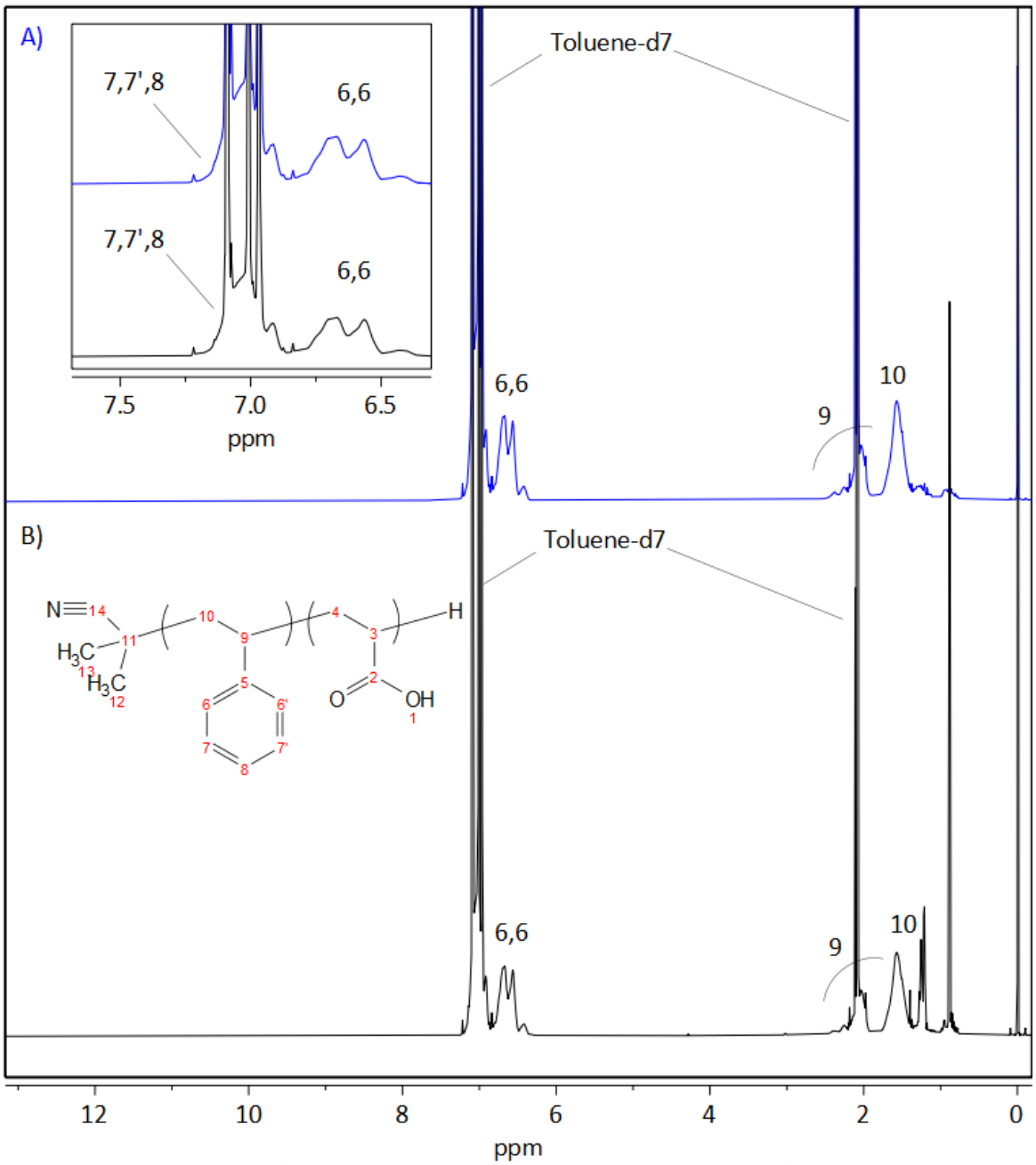

Figure S13: the ^{1}H NMR spectra of A) the PAA-*b*-PS encapsulated $CsPBBr_3$ NCs micelles and B) empty PAA-*b*-PS, in toluene-d_8. The inset shows the aromatic region expanded. Broad aromatic peak corresponding to signals 7,7' and 8 of PS moiety of polymer, is clear distinguishable from not deuterated residual Tolene-d8 peaks (sharp).

Stability tests using various additive molecules

To understand the role of the additive molecules, we initially prepared PAA-*b*-PS encapsulated $CsPbBr_3$, $Cs_{0.5}FA_{0.5}PbBr_3$ and $FAPbBr_3$ NCs by using two different organic molecules as additives, namely phenethylammonium bromide (PEABr, one functional group: ammonium) and 5-aminopentanoic acid (APAc, two functional groups: one carboxylic, one amino) and tested their stability against methanol. Freshly prepared samples were dispersed in methanol (under condition similar to those reported for Figure 3 of the manuscript) and the results are reported in Figure S10. The $CsPbBr_3$ and $Cs_{0.5}FA_{0.5}PbBr_3$ samples prepared using PEABr exhibit significant drop in the PL soon after their dispersion in methanol. The $FAPbBr_3$ sample suffered the most (nearly the complete loss of PL). On the other hand the samples prepared using APAc remained bright and stable in methanol. As the $FAPbBr_3$ NCs appeared to be the most sensitive to the type of molecule, we decided that an extensive search for a list of additive molecules that were good stabilizers for the polymer encapsulated NCs should be done indeed on NCs with $FAPbBr_3$ composition. The results of this search are reported in Figures S15-18).

PAA-*b*-PS encapsulated $FAPbBr_3$ NCs were prepared in the presence of various additive molecules having one, two or more functional groups, and either one aliphatic or one aromatic hydrocarbon chain, while all other reaction conditions were kept the same. Qualitative observations regarding the optical properties and stabilities of resulting PAA-*b*-PS encapsulated $FAPbBr_3$ NCs, when different additive molecules were used, are summarized in Table S4. Typical molecules that were tested include hexan-1-amine, hexanoic acid, 2-aminoethanethiol, 4-aminobutanoic acid, 5-aminopentanoic acid, (3-aminopropyl)phosphonic acid, 1,4-butandioic acid, 2-amino-3-hydroxypropanoic acid, pyrrolidine-2-carboxylic acid, 2-amino-3-methylbutanoic acid, 2-amino-5-(diaminomethylideneamino)pentanoic, 2-aminopentanedioic acid, -2-amino-3-sulfhydrylpropanoic acid, 2-amino-3-(1H-imidazol-4-yl)propanoic acid and 2-aminotertphthalic acid. Absorption and PL spectra measured in toluene dispersions are reported in Figure S15 and the photographs of the corresponding samples recorded under UV-lamp are reported in Figure S16. In toluene dispersions, the sample prepared using molecules having one amino and one thiol group (cysteine) had well defined absorption features but no PL at room temperature. Samples prepared using molecules containing one carboxylic, one thiol and one amino group or one carboxylic and two amino groups were weakly emissive (see Figure S15). Molecules containing more than one amino groups were not useful in the present case ($FAPbBr_3$ NCs), most likely due to their tendency to deprotonate the FA^+ cations, compromising the photoluminescence characteristic of corresponding samples, in agreement with previous reports.[8-9] Upon dispersing in methanol, the control sample (prepared without additive molecules) as well as the samples prepared using additive molecules with one functional group (amine, carboxylic acid and their mixture) significantly lost their PL. Notably, the sample prepared using a mixture of two additive molecules having each a single functional group attached to the hydrocarbon chain (hexan-1-amine + hexanoic acid) nearly lost its PL upon dispersion in methanol. On the other hand, the sample prepared using 5-aminopentanoic acid, which contains two functional groups (carboxylic and amino), both attached to the same hydrocarbon chain remains bright and stable. A comparison of these two latter samples shows that additive molecules containing two functional groups are much more effective than mixtures of two types of molecules each containing a single functional group. In general, the samples prepared by using molecules containing at least two or more functional groups remained bright and stable, see Figures S17-S18. The successful molecules had either all acidic (carboxylic, phosphonic) groups, or a

combination of acidic and at most one basic (such as amino) groups. Details on PL stability of PAA-*b*-PS encapsulated $FAPbBr_3$ NCs prepared by various additives molecules are summarized in Table S4.

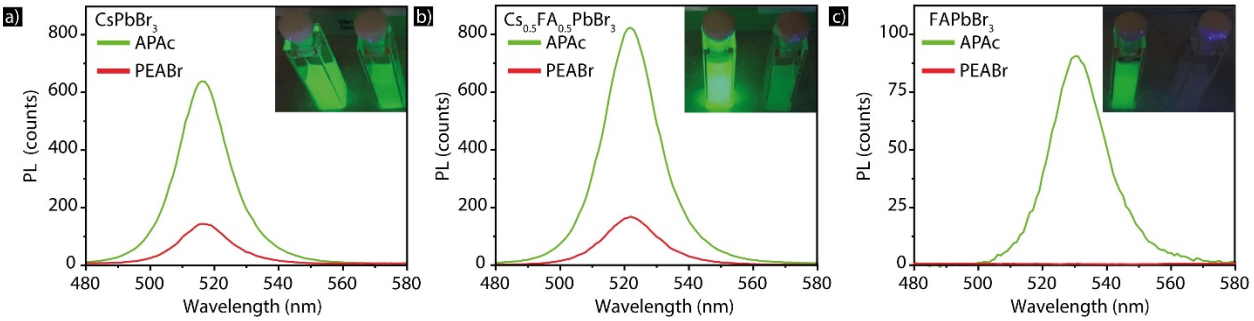

Figure S14. Stability of PAA-b-PS encapsulated NCs. (a) $CsPbBr_3$, (b) $Cs_{0.5}FA_{0.5}PbBr_3$ and (c) $FAPbBr_3$ NC samples prepared by using phenethylammonium bromide (PEABr) and 5-aminopentanoic acid (APAc) as additive molecules in methanol dispersions. The insets in panels are the photographs of the corresponding NCs samples under UV illumination (excitation, 365 nm).

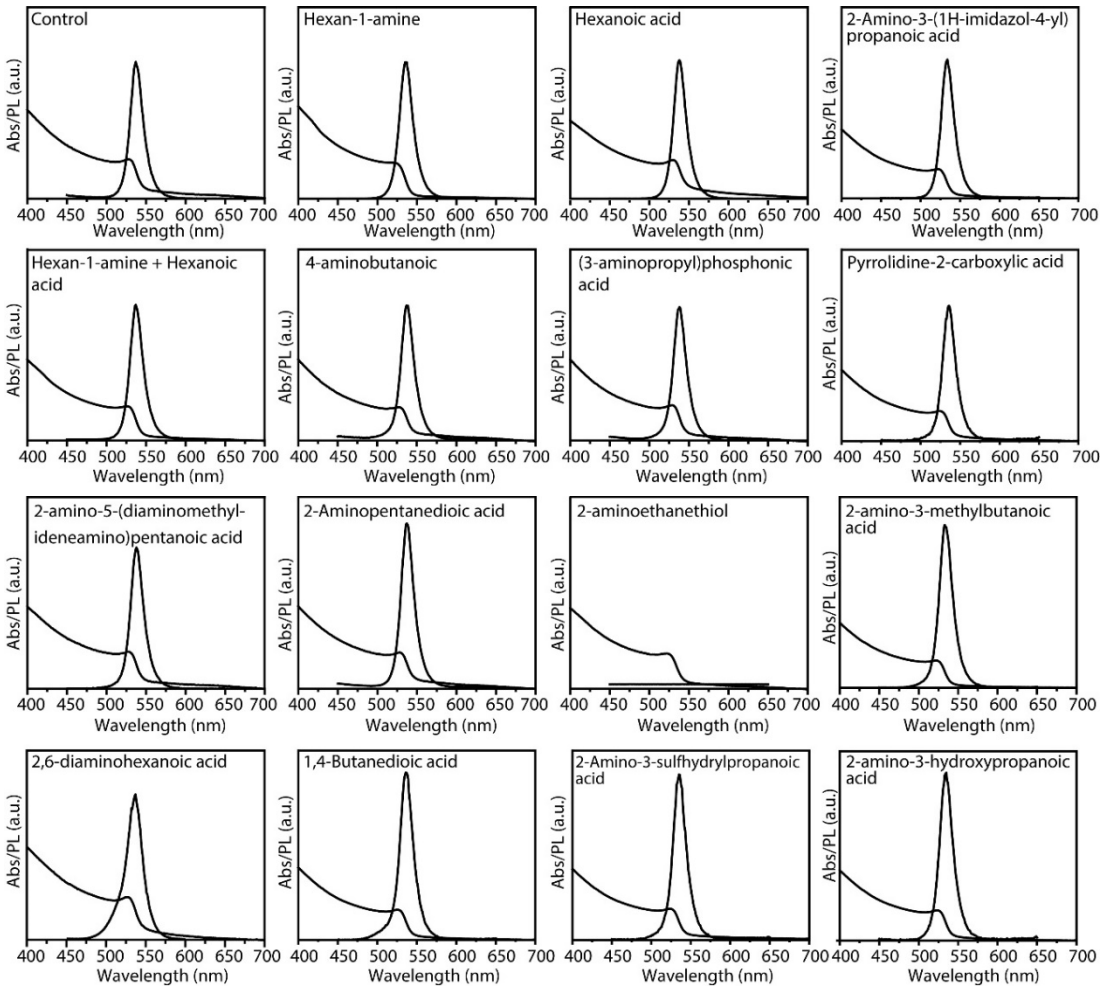

Figure S15. Synthesis of PAA-*b*-PS encapsulated $FAPbBr_3$ NCs in the presence of additive molecules with different functional groups. The control sample was prepared in the absence of additives. Optical absorption and PL spectra recorded were recorded in toluene dispersions for all the samples.

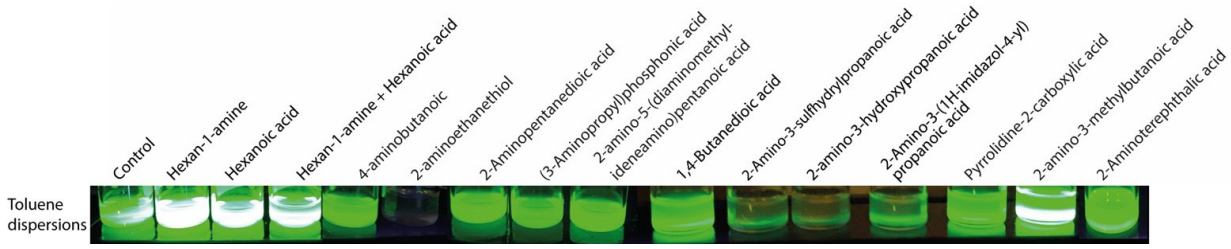

Figure S16. Photograph of PAA-*b*-PS encapsulated $FAPbBr_3$ NCs dispersions in toluene under UV illumination (excitation, 365 nm). the PL spectra of corresponding samples are reported in Figure S15.

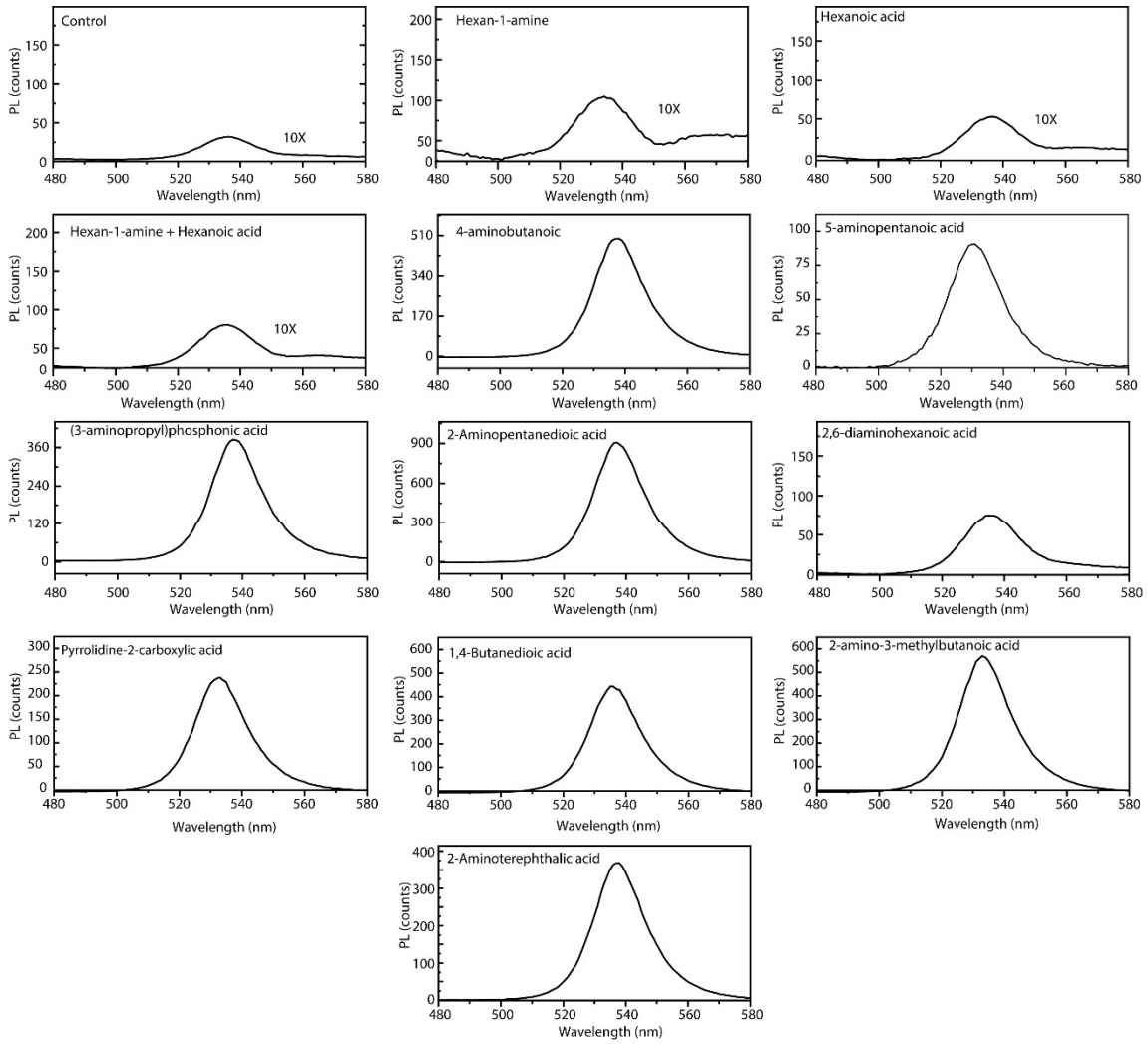

Figure S17. Stability of PAA-b-PS encapsulated FAPbBr3 NCs prepared by using additive molecules with different functional groups in methanol. PL spectra recorded on PAA-*b*-PS encapsulated $FAPbBr_3$ NCs prepared using various additive molecules (reported in Figure S15, S16) and dispersed in methanol.

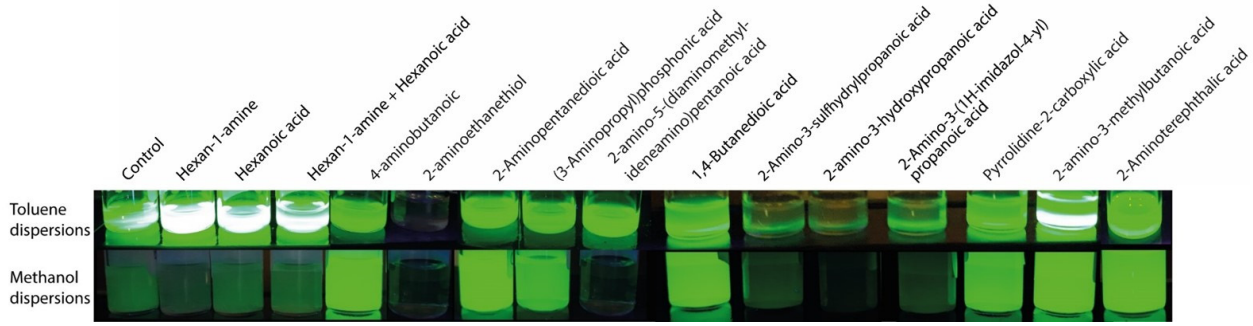

Figure S18. The photograph of PAA-*b*-PS encapsulated $FAPbBr_3$ NCs samples in toluene and methanol dispersions under UV illumination (excitation, 365 nm). The PL spectra of the samples in the corresponding solvents are reported in Figure S15 and S17.

Table S4. Optical properties of the PAA-*b*-PS encapsulated $FAPbBr_3$ NCs in terms of PL intensity and stability in toluene and methanol using different additives

Additives	Number and nature of functional group	PL in toluene dispersions [a]	PL in Methanol dispersions [b]
No additives	-	Fair	Poor
hexan-1-amine	1 (1 $-NH_2$)	High	Poor
Hexanoic acid	1 (1 –COOH)	High	Poor
hexan-1-amine + Hexanoic acid	1 (1 $-NH_2$) + 1 (1 –COOH)	High	Poor
2-aminoethanethiol	2 (1 –SH, 1 $-NH_2$)	No PL	-
4-aminobutanoic	2 (1 –COOH, 1 $-NH_2$)	High	High
5-aminopentanoic acid	2 (1 –COOH, 1 $-NH_2$)	High	High
(3-aminopropyl)phosphonic acid	2 (1 $-P(=O)(OH)_2$, 1 NH_2)	High	High
1,4-Butanedioic acid	2 (2 –COOH)	High	High
2-amino-3-hydroxypropanoic acid	2 (1 –COOH, 1 -NH_2)	Poor	No PL
Pyrrolidine-2-carboxylic acid	2 (1 –COOH, 1 –NH-)	High	High
2-amino-3-methylbutanoic acid	2 (1 –COOH, 1 -NH_2)	High	High
2-amino-5-(diaminomethylideneamino)pentanoic acid	2 (1 –COOH, 1 Formamidine)	High	No PL
2-Aminopentanedioic acid	3 (2 –COOH, 1 -NH_2)	High	High
2-Amino-3-sulfhydrylpropanoic acid	3 (1 –COOH, 1 -NH_2, 1 –SH)	Poor	No PL
2-Amino-3-(1H-imidazol-4-yl)propanoic acid	3 (1 –COOH, 1 $-NH_2$, 1 Imidazole)	Poor	Poor
2-aminotertphthalic acid	3 (2 –COOH, 1 $-NH_2$)	High	High

[a,b] The sample were marked as Fair, poor and high based on their PL intensity in toluene and methanol dispersions. We used PAA-*b*-PS encapsulated $FAPbBr_3$ (5-aminopentanoic acid as additive) as a reference sample for the comparison of relative PL intensity. This sample has a PLQY of 61% and marked as "high" in terms of PL intensity. The samples prepared by using various additive molecules with the PL intensity at least 80% or above compared to the reference sample were considered as "high". On the other hand, the samples with PL intensity below 30% compared to the reference sample were classified as "poor". The samples having the PL intensity in the range of 30-80 % were considered as "fair". For the stability in methanol, the samples retaining 50 % of their PL compared to their starting PL in toluene dispersion were considered as "high". The samples losing more than 90% of their PL intensity upon dispersion in methanol were considered as "poor" and the samples with PL intensity within these extremes were considered as "fair".

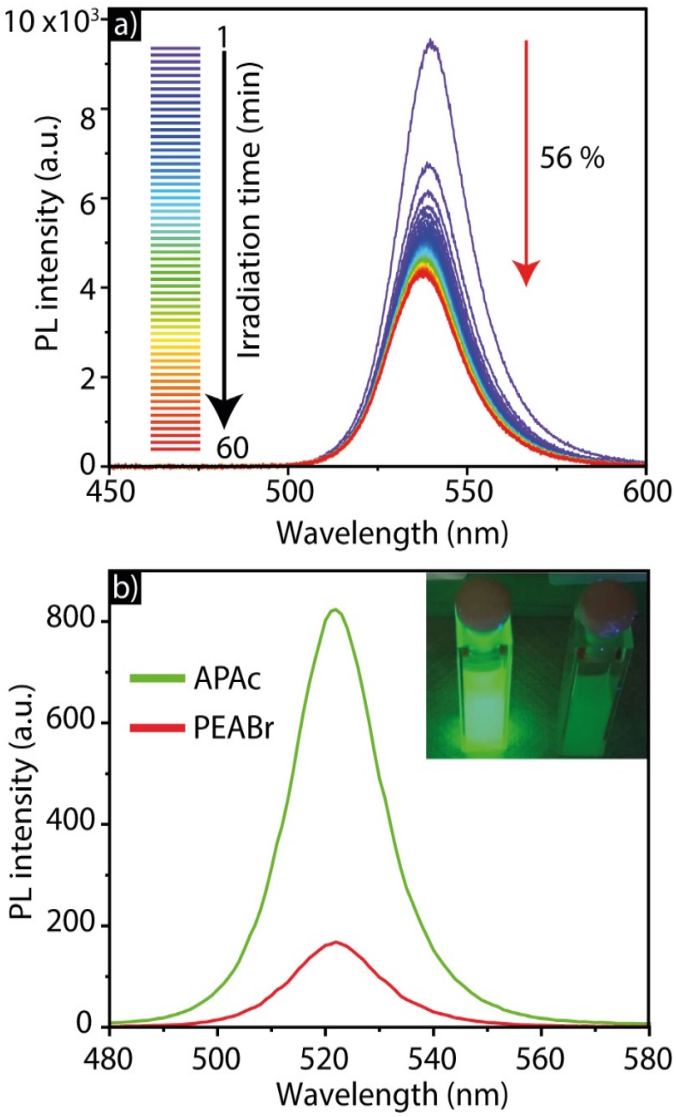

Figure S19: Stability of $Cs_{0.5}FA_{0.5}PbBr_3$ NCs prepared using two different additive molecules. (a) Evolution of PL spectra of NCs prepared by using phenethylammonium bromide (PEABr) showing 56 % loss of PL over 60 min of continuous exposure to laser irradiation. While instead, the samples prepared by using 5-aminopentanoic acid (APAc) evidenced 6% loss of PL for the same period of exposure to laser irradiation (see Figure 4d of the main text). Panel (b) shows the stability of both samples in methanol dispersions. The inset in panel (b) corresponds to the photograph of the same samples under UV illumination (excitation, 365 nm).

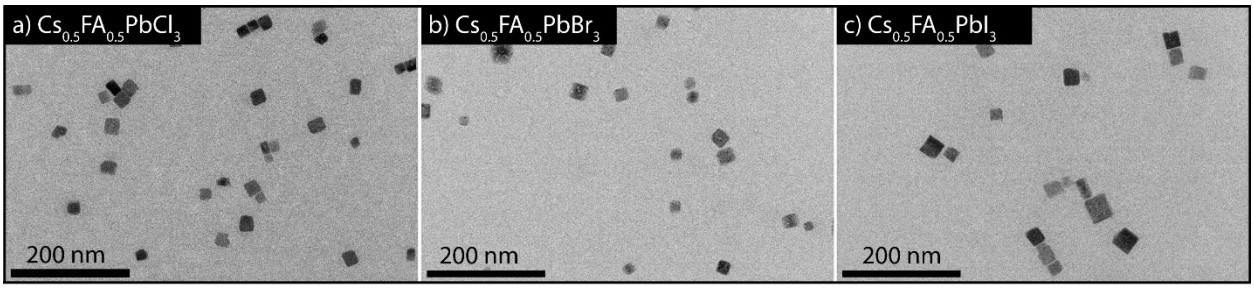

Figure S20: Representative TEM images of PAA-*b*-PS encapsulated NCs. (a) $Cs_{0.5}FA_{0.5}PbCl_3$, (b) $Cs_{0.5}FA_{0.5}PbBr_3$ and (c) $Cs_{0.5}FA_{0.5}PbI_3$ NCs deposited from toluene dispersions. $Cs_{0.5}FA_{0.5}PbCl_3$ and $Cs_{0.5}FA_{0.5}PbI_3$ NCs were prepared by halide exchange reactions starting from $Cs_{0.5}FA_{0.5}PbBr_3$ NCs.

Additional data on emitting powders and on the white light emitting layer preparation

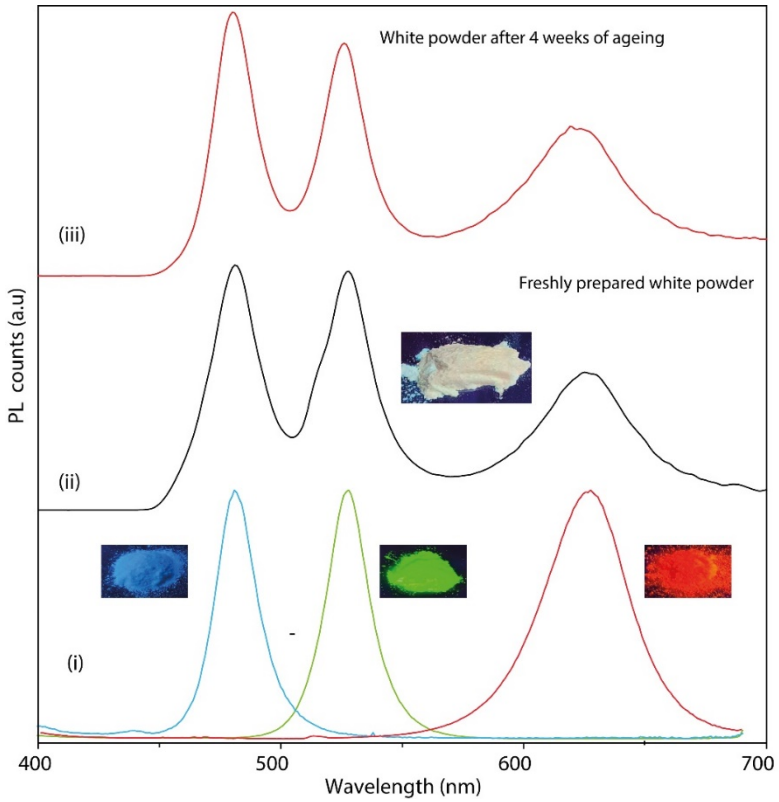

Figure S21: Comparison of the spectral features of PAA-*b*-PS encapsulated $Cs_{0.5}FA_{0.5}PbX_3$ NCs powders before (i) and after mixing (ii), evidencing the retention of their native PL peak position in the white emitting blend. A PL spectrum recorded the same powder mixture after 4 weeks of ageing under ambient air shows that the PL peak positions and relative PL intensities remain unchanged (iii). The insets correspond to the photographs of the various samples under UV illumination (excitation light at 365 nm).

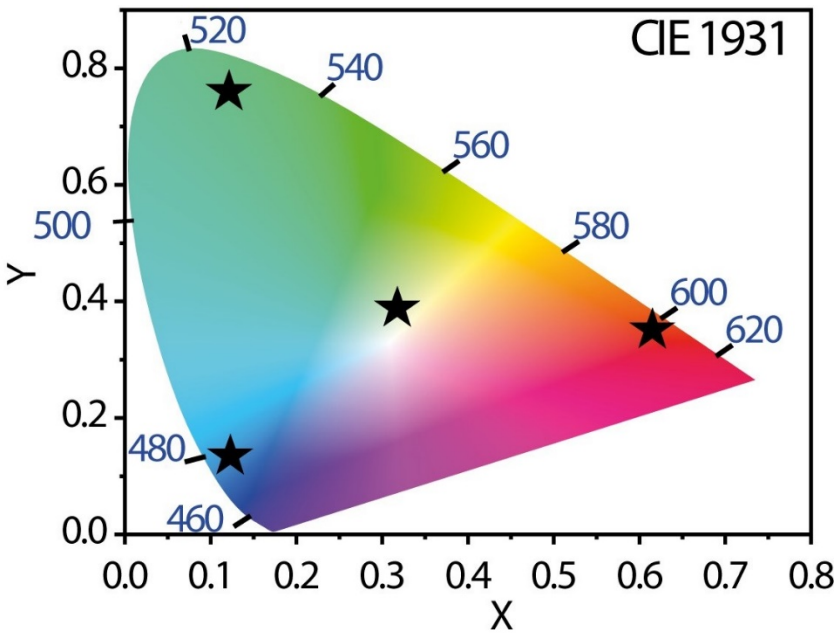

Figure S22: CIE 1931 diagram of the white emitting mixture of powders and the respective components reported in Figure 6 and Figure S16.

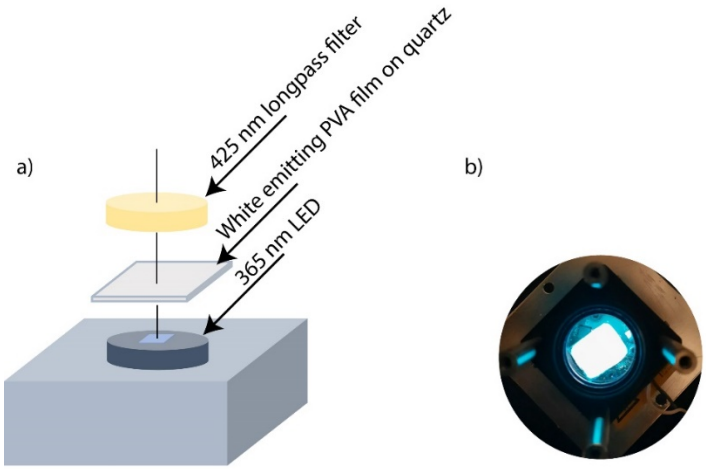

Figure S23: a) Schematic illustration of the device structure used for the fabrication of a white light-emitting device based on a UV-LED for excitation, a PVA film embedding the NCs and long pass filter. Panel (b) is a photograph of the white emitting device under operational conditions.

References

1. Akkerman, Q. A.; Martínez-Sarti, L.; Goldoni, L.; Imran, M.; Baranov, D.; Bolink, H. J.; Palazon, F.; Manna, L., Molecular Iodine for a General Synthesis of Binary and Ternary Inorganic and Hybrid Organic–Inorganic Iodide Nanocrystals. *Chem. Mater.* **2018,** *30* (19), 6915-6921.
2. Zhang, J.; Jiang, P.; Wang, Y.; Liu, X.; Ma, J.; Tu, G., In-situ Synthesis of Ultrastable $CsPbBr_3$ Perovskite Nanocrystals Coated with Polyimide in a CSTR System. *ACS Appl. Mater. Interfaces* **2019,** *12*, 3080-3085.
3. Protesescu, L.; Yakunin, S.; Bodnarchuk, M. I.; Krieg, F.; Caputo, R.; Hendon, C. H.; Yang, R. X.; Walsh, A.; Kovalenko, M. V., Nanocrystals of cesium lead halide perovskites ($CsPbX_3$, X= Cl, Br, and I): novel optoelectronic materials showing bright emission with wide color gamut. *Nano Lett.* **2015,** *15* (6), 3692-3696.
4. Hou, S.; Guo, Y.; Tang, Y.; Quan, Q., Synthesis and stabilization of colloidal perovskite nanocrystals by multidentate polymer micelles. *ACS Appl. Mater. Interfaces* **2017,** *9* (22), 18417-18422.
5. Hintermayr, V. A.; Lampe, C.; Löw, M.; Roemer, J.; Vanderlinden, W.; Gramlich, M.; Böhm, A. X.; Sattler, C.; Nickel, B.; Lohmüller, T., Polymer nanoreactors shield perovskite nanocrystals from degradation. *Nano Lett.* **2019,** *19* (8), 4928-4933.
6. He, Y.; Yoon, Y. J.; Harn, Y. W.; Biesold-McGee, G. V.; Liang, S.; Lin, C. H.; Tsukruk, V. V.; Thadhani, N.; Kang, Z.; Lin, Z., Unconventional route to dual-shelled organolead halide perovskite nanocrystals with controlled dimensions, surface chemistry, and stabilities. *Sci. Adv.* **2019,** *5* (11), eaax4424.
7. Liu, Y.; Wang, Z.; Liang, S.; Li, Z.; Zhang, M.; Li, H.; Lin, Z., Polar Organic Solvent-Tolerant Perovskite Nanocrystals Permanently Ligated with Polymer Hairs via Star-like Molecular Bottlebrush Trilobe Nanoreactors. *Nano Lett.* **2019,** *19* (12), 9019-9028.
8. Protesescu, L.; Yakunin, S.; Bodnarchuk, M. I.; Bertolotti, F.; Masciocchi, N.; Guagliardi, A.; Kovalenko, M. V., Monodisperse formamidinium lead bromide nanocrystals with bright and stable green photoluminescence. *J. Am. Chem. Soc.* **2016,** *138* (43), 14202-14205.
9. Imran, M.; Caligiuri, V.; Wang, M.; Goldoni, L.; Prato, M.; Krahne, R.; De Trizio, L.; Manna, L., Benzoyl halides as alternative precursors for the colloidal synthesis of lead-based halide perovskite nanocrystals. *J. Am. Chem. Soc.* **2018,** *140* (7), 2656-2664.